2007-12

Neural Dynamics Underlying Impaired Autonomic and Conditioned Responses Following Amygdala and Orbitofrontal Lesions

Neural Dynamics Underlying Impaired Autonomic and Conditioned Responses Following Amygdala and Orbitofrontal Lesions

Stephen Grossberg, Daniel Bullock, and Mark R. Dranias[1]

Department of Cognitive and Neural Systems,
Center for Adaptive Systems
and
Center of Excellence for Learning in Education, Science, and Technology
Boston University
677 Beacon St., Boston, MA 02215

Submitted December, 2007
CAS/CNS Technical Report 2007-026

Corresponding author: Stephen Grossberg
Phone: 617-353-7858 or -7857
FAX: 617-353-7755
Email: steveg@bu.edu

Acknowledgements
S.G. was supported in part by the National Science Foundation (NSF SBE-0354378) and the Office of Naval Research (ONR N00014-01-1-0624). M.D. was supported in part by the Defense Advanced Research Projects Agency and the Office of Naval Research (ONR N00014-95-1-0409), the National Institutes of Health (NIH R29-DC02952), the National Science Foundation (NSF IIS-97-20333 and NSF SBE-0354378), and the Office of Naval Research (ONR N00014-01-1-0624). D.B. was supported in part by the National Institutes of Health (NIH R01-DC007683) and the National Science Foundation (NSF SBE-0354378).

[1] Names are in rotated alphabetical order

ABSTRACT
A neural model is presented that explains how outcome-specific learning modulates affect, decision-making and Pavlovian conditioned approach responses. The model addresses how brain regions responsible for affective learning and habit learning interact, and answers a central question: What are the relative contributions of the amygdala and orbitofrontal cortex to emotion and behavior? In the model, the amygdala calculates outcome value while the orbitofrontal cortex influences attention and conditioned responding by assigning value information to stimuli. Model simulations replicate autonomic, electrophysiological, and behavioral data associated with three tasks commonly used to assay these phenomena: Food consumption, Pavlovian conditioning, and visual discrimination. Interactions of the basal ganglia and amygdala with sensory and orbitofrontal cortices enable the model to replicate the complex pattern of spared and impaired behavioral and emotional capacities seen following lesions of the amygdala and orbitofrontal cortex.

KEYWORDS: Pavlovian conditioning, inferotemporal and rhinal cortex, amygdala, basal ganglia, orbitofrontal cortex

INTRODUCTION

Animals exploit their environments by identifying and acquiring resources that fulfill their metabolic needs. When multiple options are available, animals must often rank and decide among available options. Discriminating, evaluating, and selecting goals requires the interaction of cognitive, emotional, motor, and reinforcement learning systems. Cognitive systems enable animals to identify cues and predict likely outcomes; emotional systems assign value and motivated attention to cues, aiding decision-making; reinforcement learning systems strengthen, among others, stimulus and response associations that lead to the procurement of reward.

Consuming a reward activates neural circuits that respond to the sensory, affective, and drive properties of the unconditioned stimuli (US). When stimuli and responses are paired with rewards, associations form that allow these stimuli and responses to recall information about the sensory, affective, and drive properties of predicted rewards (Grossberg, 1972; Rescorla, 1991; Dickinson and Balleine, 2001; Cardinal et al., 2002). When a stimulus or response activates the representation of an outcome with which it has been previously paired, the representation is not merely a passive record of previous experience. Rather, it carries information about the current desirability of outcomes and can be used to reorder preferences for cues and behavioral plans (Davidson et al., 1997; Hall, 2001; Cardinal et al., 2002). Without such reorderings based on the current values of predicted outcomes, conditioned responding can become rigid and guided only by the prior history of reward that is implicitly encoded in the learned strength of stimulus-response links that are assumed to underlie habits (Rescorla, 1991; Dickinson and Balleine, 2001).

The ability of stimulus-outcome associations to override habit and influence response vigor, emotional arousal, and decision-making behavior depends crucially on the interactions of the amygdala and orbitofrontal cortex (Malkova et al., 1997; Gallagher et al., 1999; Hatfield et al., 1996; Braesicke et al., 2005). In order to understand how outcome-specific information is encoded and used to alter decision-making, affect, and Pavlovian conditioned responding, we developed a neural network model capable of explaining behavioral and neural variations observed in three basic tasks: consumption of a food US (unconditioned stimulus), Pavlovian conditioning of a CS (conditioned stimulus) that predicts a US, and simultaneous visual discrimination (SVD).

Experimental tasks such as the food consumption task are useful for probing how the current value of food rewards is computed in the brain. Variations in food consumption provide insight into how such computations regulate the motivation to consume specific foods. *Food specific satiety* (FSS) is exemplified by such phenomena as the "dessert effect": Someone who has eaten one food, say turkey, to the point of satiation, will nevertheless continue to eat if offered a second food, say ice cream. More generally, FSS encompasses the class of phenomena in which a normally effective Pavlovian US, such as meat or juice, becomes progressively less valuable, relative to alternatives, as it is consumed (Rolls and Rolls, 1997).

Pavlovian conditioning of a CS paired with a US provides opportunities to study how outcome-specific revaluations (as in FSS) can alter Pavlovian conditioned responses (CRs); e.g., "autoshaped" approach responses. The value of a Pavlovian CS, as measured by the vigor and frequency of CS-induced approach responses, reflects the current value of the associated US (Davidson et al., 1997; Hatfield et al., 1996). Notably, as a result of stimulus-outcome associations learned during conditioning, Pavlovian CSs and CRs will 'automatically' revalue to reflect a change in US value, whether it is effected by deprivation or satiation, and even if no additional CS-US pairings occur during the US revaluation (Dickinson and Balleine, 2001;

Cardinal et al., 2002). In marked contrast, the value of higher-order CSs does not automatically track shifts in US value and must be re-exposed to the US if they are to reflect changes in US value due to deprivation or satiation (Balleine et al., 1995; Balleine and Dickinson, 1998).

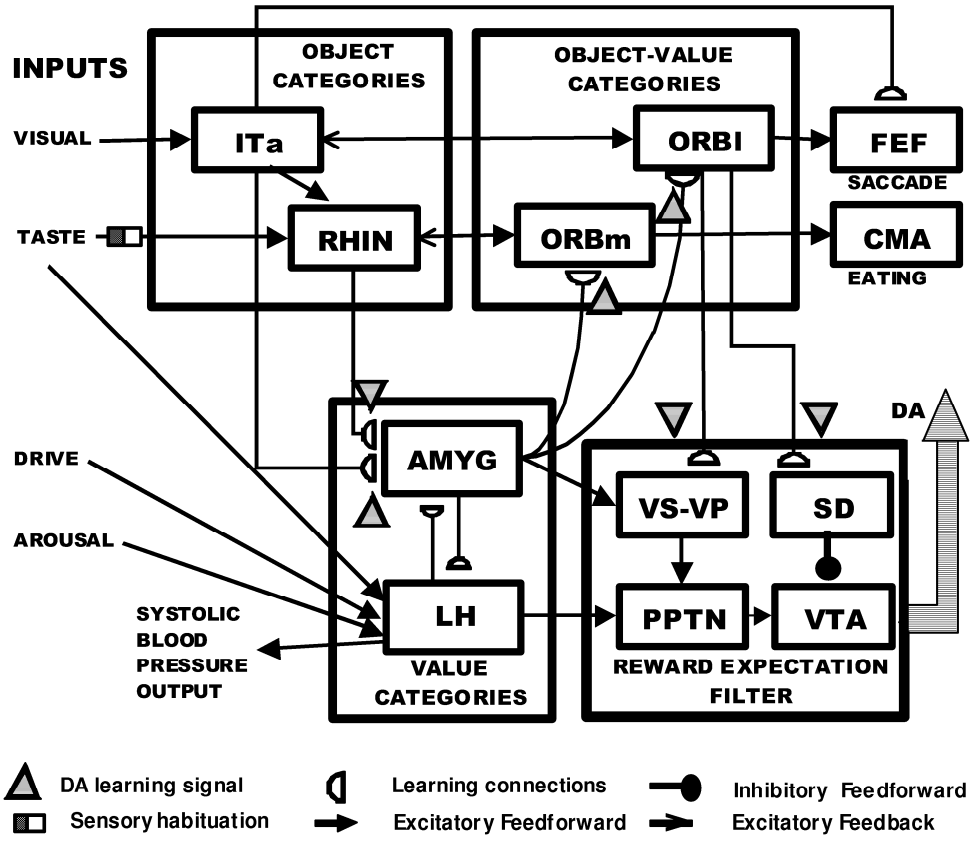

Figure 1: MOTIVATOR model circuitry. The model receives four types of inputs: visual, gustatory, drive (metabolite-related signals), and arousal. The model generates eye movements via the frontal eye fields (FEF), food consumption responses via cortical masticatory area (CMA), emotional outputs (systolic blood pressure) via lateral hypothalamic output cell (LH_out) projections to the brainstem, adn dopamine outputs from the substantia nigra/ventral tegmental area (SNc/VTA). Other brain regions simulated include the anterior inferotemporal cortex (ITa), rhinal cortex (RHIN), lateral orbitofrontal cortex (ORBl), medial orbitofrontal cortex (ORBm), amygdala (AMYG), lateral hypothalamus (LH), ventral striatum (VS), ventral pallidum (VP), striosomes of the striatum (SD), and the pedunculopontine nucleus (PPTN). See text for further details.

In simultaneous visual discrimination (SVD), animals use saccades to choose, from an array of stimuli (usually two), the stimulus that predicts the most preferred reward. Thus SVD can be used to assay the role that predicted outcome information plays in decision-making. Reward-related information influences both decision time and stimulus selection (Malkova et al., 1997; Roesch and Olson, 2004). In the usual SVD paradigm, a reversal of preference occurs after exposure to multiple trials with a reversed CS-response-outcome contingency (Jagadeesh et al., 2001; Brown et al., 2004). However, US devaluation also causes a reliable reversal of stimulus preference and does so without the need for any additional exposures to CS-saccade-US sequences after the revaluation (Malkova et al., 1997; Balleine and Dickinson, 1998). This is consistent with the principle stated above because stimulus-outcome associations, crucial for

revaluation and guiding saccadic choice in the SVD task, are learned via CS-US pairings, during which saccadic CRs emerge by autoshaping.

To understand how the mammalian brain learns to perform these tasks, we have developed a computational neural model, shown in Figure 1, called MOTIVATOR: **M**atching **O**bjects **T**o **I**nternal **VA**lues **T**riggers **O**ption **R**evaluations. The MOTIVATOR model simulates how an animal processes stimuli in parallel, assesses whether these stimuli are predictive of rewards that match its current needs, and then uses this information to select preferred targets for action while suppressing responses to less preferred and irrelevant stimuli. The model has been briefly reported in Dranias et al. (2007a, 2007b).

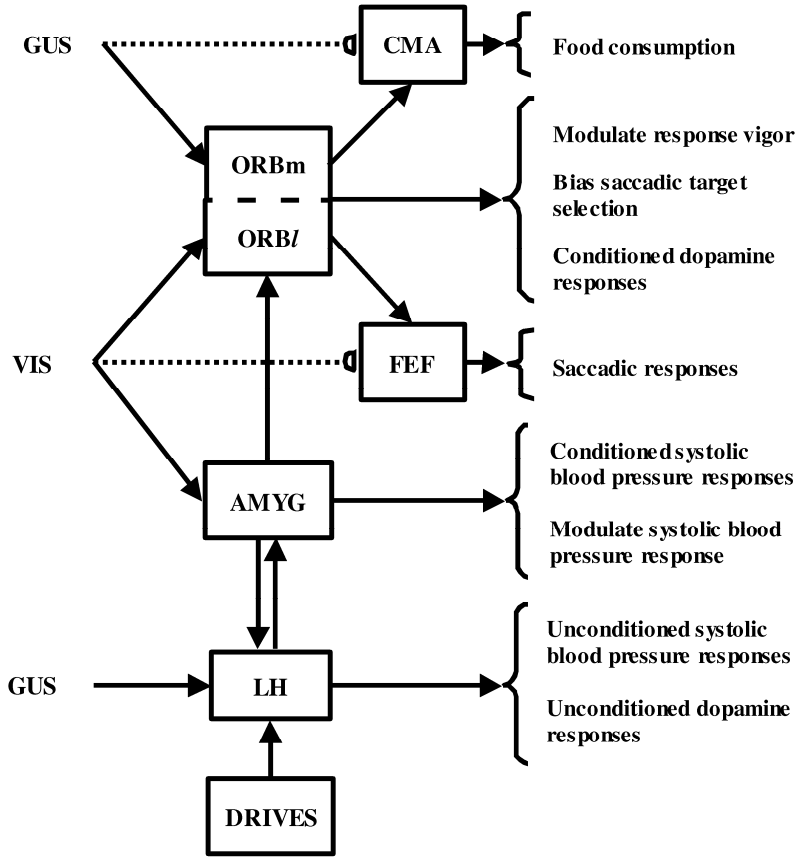

Figure 2: A neural axis mediating the effects of deprivation/satiation on five classes of stimulus-evoked responses. Gustatory inputs (GUS) are elicited by the consumption of an unconditioned stimulus (US). GUS inputs automatically elicit unconditioned responses via pathways linking GUS with the LH and the cortical masticatory area (CMA). Unconditioned responses elicited by the LH consist of an autonomic response (change in systolic blood pressure (BP)) and a dopamine response (rewards elicit a burst in activity). Drive inputs and habituative GUS inputs (half-shaded boxes indicate use-dependent habituation) allow the LH to be sensitive to the current motivational value of specific outcomes. Feeding responses are regulated by the CMA and modulated by ORB_m activity. Visual inputs (VIS) of conditioned stimuli excite the frontal eye fields (FEF) and elicit conditioned responses that are sensitive to outcome specific information via the AMYG and ORB_l. Conditioned responses elicited by the AMYG include conditioned autonomic responses (changes in BP). The AMYG modulates the intensity of conditioned autonomic responses in an outcome-specific fashion. The AMYG interacts with the LH to calculate outcome specific value. Conditioned responses to visual stimuli are elicited through the FEF while ORB_l signals modulate the vigor of Pavlovian autoshaping responses and bias saccade target selection through the FEF. ORB_l signals elicit conditioned dopamine responses via a learned pathway to the ventral striatum (VS) (see Fig. 1).

In MOTIVATOR, the learning/extinction that occurs at several sites responds to the statistics implicit in exposures to CS-US contingencies, and is modulated by dopaminergic signals emerging from an incorporated prior model of basal ganglia function (Brown et al., 1999). Figure 2 illustrates how the model relates a three-level *evaluative neuraxis*, including lateral hypothalamus (LH), amygdala (AMYG), and orbitofrontal cortex (ORB), to the motivational regulation of seven classes of stimulus-evoked responses, including US-evoked food consumption, autoshaped CS-guided saccadic orienting responses, US-evoked and CS-evoked dopamine responses, and US-evoked and CS-evoked changes in autonomic responses, notably systolic blood pressure. The LH processes the motivational value of USs and modulates the vigor of URs (unconditioned responses) so that they reflect current US value. The AMYG receives CS inputs, calculates the values of prospective outcomes predicted by those CSs, and enables CSs to activate the LH and elicit autonomic CRs. The ORB_l (lateral ORB) uses inputs from AMYG to assign current reward value to internal representations of predictive CSs, thus biasing target selection in saccadic tasks and enhancing the vigor of Pavlovian CRs. The basal ganglia act as a reward expectation filter, generating dopaminergic signals whenever an unexpected reward occurs or when an expected reward is omitted. Dopamine signals help adjust links along the Figure 2 neuraxis.

Simulations of MOTIVATOR are used to address basic issues such as how the habit and emotional systems interact and whether the amygdala or orbitofrontal cortex is responsible for the calculation of outcome value. Simulated lesion studies demonstrate the consequences of model hypotheses for affect, Pavlovian conditioned responding, and decision-making.

METHODS

Tasks

Using three basic tasks, nine experiments were simulated: (1) US Task; (2) impact of food specific-satiety (FSS) on the US Task; (3) CS Task; (4) impact of FSS on the CS Task; (5) SVD task; (6) SVD task comparing reaction times with different reward magnitudes; (7) impact of FSS on the SVD task; (8) A variant of the SVD task examining how FSS impacts the choice between stimuli associated with different reinforcers; and (9) Second order conditioning (SOC) task. Intact, amygdala-lesioned ('AX'), and orbitofrontal-lesioned ('OX') models were simulated in each experiment.

The timing of the food consumption or US task (Figure 3A) is taken from Ono et al. (1986). Three inputs are presented during simulations of the US task, a gustatory input (GUS), a hunger or metabolite level input (DRIVE), and an arousal level input (AROUSAL). GUS inputs are gated by a sensory habituation term (HAB) that represents sensory-specific satiety and decays in proportion to food consumption. Arousal inputs, α_1, to LH cells were normally set to 0.5. Outputs include a food consumption signal generated by cortical masticatory areas (CMA), dopamine bursting responses generated in the SNc/VTA (Figures 3N and 3O), and a systolic blood pressure signal (BP) that scales with emotional state (Figures 4D and 4E).

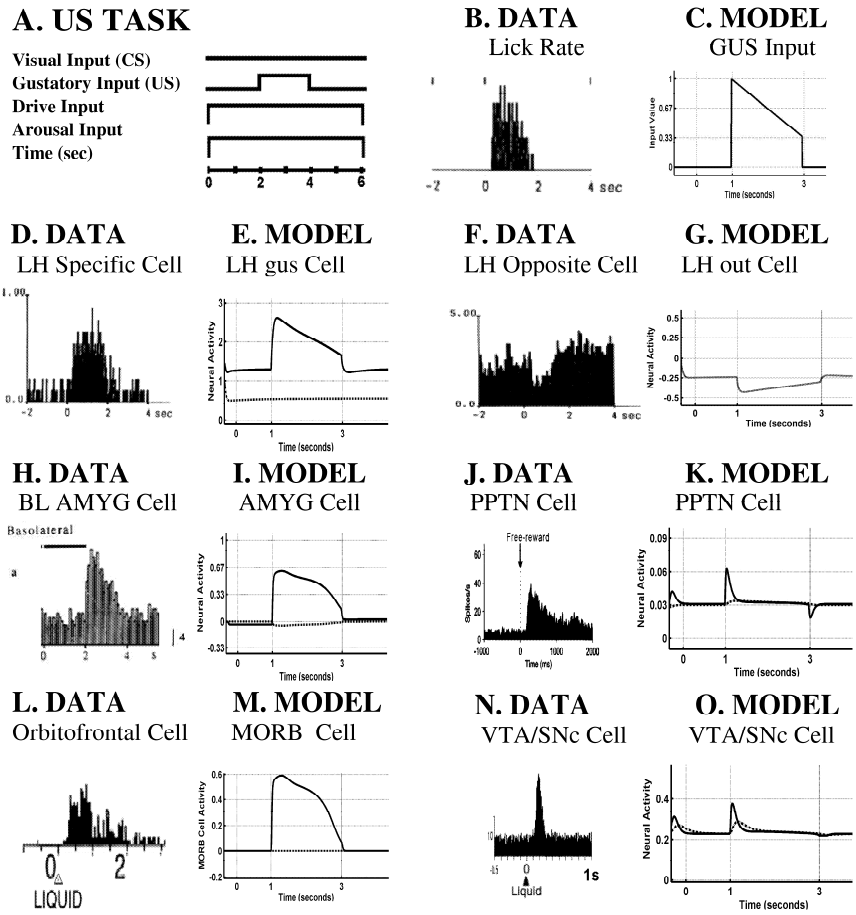

Figure 3: US task timing and cell responses. (A) Input timing in the US Task. Food reward presentation is simulated by a two second presentation of a gustatory input. No visual input is presented. Drive and Arousal inputs are constant throughout the task. During devaluation trials, some drive and taste inputs are decreased to simulate food-specific satiety. (B) Licking rate during US Task (reprinted with permission from Ono et al., 1986). (C) Model gustatory inputs mimic typical licking rates. (D) Response of lateral hypothalamic cell to sweet taste reflects motivational value (reprinted with permission from Ono and Nakamura, 1985). (E) Model LH gustatory cells respond to specific tastes and correlated metabolic inputs. (F) Lateral hypothalamic opposite cell responds to the presentation of glucose with inhibition (reprinted with permission from Ono and Nakamura, 1985). (G) Model aversive LH output cell responds with inhibition to a sweet gustatory input. (H) Basolateral amygdala cell responds to the consumption of a glucose reward (reprinted with permission from Muramoto et al., 1993). (I) Model AMYG US drive value category cell responds to gustatory inputs. (J) Pedunculopontine Nucleus cells respond to free reward presentation (Reprinted with permission from Kobayashi et al., 2002). (K) Model PPTN cell responds to gustatory inputs. (L) Reward-responsive orbitofrontal cell (reprinted with permission from Tremblay and Schultz, 2000). (M) Model ORB_m cell responds to gustatory inputs. (N) Response of dopamine cell to unsignaled juice reward (reprinted with permission from Mirenowicz and Schultz, 1994). (O) Model SNc/VTA cell generates dopamine response to unexpected reward.

Two experiments were simulated as part of the US task. The first experiment examined model responses when DRIVE inputs were high and uniform. Food inputs are composed of a binary combination of five basic GUS inputs: sweet, salty, savory, bitter, and fatty. Food 1 was salty and sweet, Food 2 was savory and fatty, and Food 3 was savory and sweet. DRIVE inputs coded sugar, fat, salt, or amino acid levels. The second experiment assayed how food-specific satiety devalues consumption. For the US devaluation task, DRIVE inputs and the initial value for HAB were reduced to reflect food specific satiety for 'Food 2' (for a discussion of the dynamics

of US task performance, see Supplementary Notes 1). In particular, salty and sweet tastes were habituated and DRIVE inputs associated with salt and glucose reduced. In the AMYG-lesion case, dopamine-gated learning and sensory-specific habituation allow RHIN cells to activate CMA PRCO cells in a manner that preserves FSS. Following ORB_m lesions, RHIN cell inputs to the CMA are preserved and drive food consumption behavior (Huang et al., 1989). A direct path from the AMYG to the CMA also exists (Hatanaka et al., 2000).

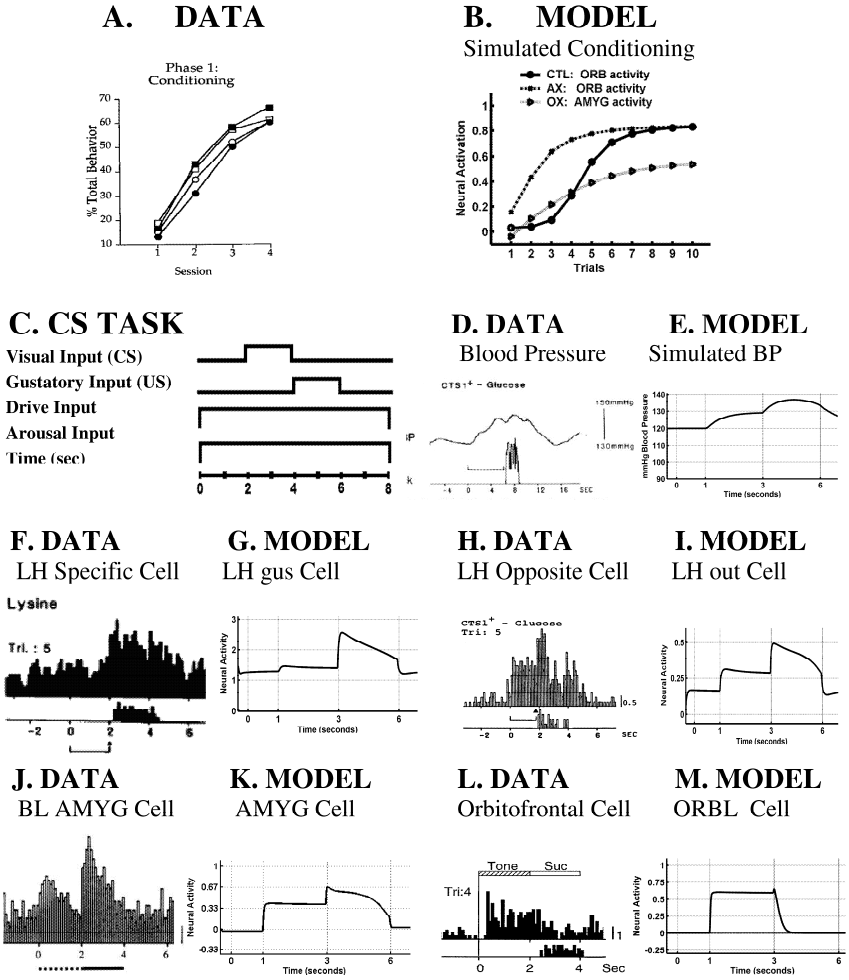

Figure 4: CS Task training and cell responses. (A) Pavlovian conditioning, is not impaired by sham (open circles) and orbitofrontal lesions (closed squares; reprinted with permission from Gallagher et al. 1999). (B) Model simulates Pavlovian conditioning (CTL; closed circles), and is not impaired by lesions of model AMYG (AX; '+' sign), or ORB (OX; triangles). ORB_l activity measures frequency of conditioned responses for CTL and AX; for OX case AMYG activity measures conditioned response frequency. (C) The visual stimulus is presented for 2 seconds and then immediately afterwards the gustatory input is presented for 2 seconds (Ono et al., 1986). In simulations of the CS task, Drive and Arousal inputs remain constant. (D) Mean systolic blood pressure response during CS task (reprinted with permission from Nakamura et al., 1992). (E) Systolic blood pressure output. (F) Taste-specific LH cell (reprinted with permission from Torii et al., 1998). (G) Model LH gus cell responds in a taste, drive, and CS-sensitive fashion. (H) LH opposite cell responds similarly to glucose taste and a glucose-related CS (reprinted with permission from Ono et al., 1986). (I) Model appetitive LH output cells respond with excitation to sweet gustatory inputs and conditioned stimuli associated with glucose. (J) Basolateral amygdala cell responds to glucose and CS associated with glucose (reprinted with permission from Muramoto et al., 1993). (K) Model AMYG US drive value category cell selectively responds to conditioned stimuli and reflects expected value of US. (L) Stimulus-selective orbitofrontal cell (reprinted with permission from Yonemori et al., 2000). (M) Model ORB_l cell reflects incentive value and responds in a stimulus-selective fashion to CS.

The CS task simulates data from the Pavlovian food-cup approach task reported by Gallagher et al. (1999). To ensure that simulation results can be directly compared with electrophysiological data, the timing of the CS task (Figure 4A) is taken from Ono et al. (1986). In the CS task, DRIVE, AROUSAL, visual (VIS), and GUS inputs are presented. The visual input (VIS) is presented for two seconds, followed immediately by the presentation of a food reward for two seconds (GUS input). Outputs include the systolic BP signal that reflects affect and LH activation, FEF activity to generate a conditioned approach signal, and dopamine signals via the SNc/VTA. The CS task was simulated in two conditions: sated and unsated. In the unsated case, DRIVE inputs were set to uniformly high values. AROUSAL inputs were constant unless activated by a reward omission signal from the basal ganglia. The reward omission signal occurred whenever the cortical dopamine dip (D_2) signal falls below a threshold value of 0.2. Arousal inputs burst, increasing six fold when this happens.

For the second, sated, case food rewards were devalued in an outcome-specific fashion (for a discussion of the dynamics of CS task performance see Supplementary Notes 2). In particular, Food 1 was devalued again and DRIVE inputs and the HAB initial value were reduced to reflect food-specific satiety. Each trial was associated with a behavioral output consisting of the occurrence or non-occurrence of a Pavlovian conditioned response. A Pavlovian response was generated whenever FEF activity exceeded a threshold value, which was chosen to be 0.3. Only one response was counted in each trial. In the following discussion, both AMYG-lesion and ORB-lesion cases, FEF activity, response vigor, and selectivity were solely determined by inputs from the IT_a that had been trained using dopamine-gated adaptive weights and stimulus-response learning.

The SVD task is a two-alternative forced choice task where one of two differentially rewarded stimuli is selected by making a saccade. In order to compare model simulations with electrophysiological data, the timing of the SVD task (Figure 5A) was taken from Jagadeesh et al. (2001). Autonomic output is measured using the BP signal, SNc/VTA activity generates a dopamine signal, and saccades are executed based on CS-selective activity in the FEF. CS-selective activity in the ORB_l relays incentive salience and incentive motivational signals from the AMYG to the IT_a and FEF (Figure 1). Incentive salience enhances the representation of attractive stimuli and incentive motivation speeds saccadic reactions (Brown et al., 2004). The saccadic response is generated in the FEF in response to signals from the ORB_l and IT_a. In general, the cue associated with the strongest ORB_l signal is selected as the target for a saccade. Target selection occurs between 300ms and 450ms and an unselected cue is terminated at 450ms.

Saccadic reaction times are reported for simulations involving simple SVD trials where the rewarded cue is discriminated from an unrewarded cue. The saccadic reaction time was determined by using a summation-to-threshold decision rule (Schall and Thompson, 1999). The first FEF cell to exceed the fixed threshold generated a saccade to its preferred stimulus. A threshold of 150 cumulative units was selected to elicit a saccade. When motivation is high, saccadic responses in the FEF are determined by ORB_l cell activity, which represents the expected value of competing stimuli. To break ties and ensure saccades are elicited when motivation levels are low, FEF cells also receive a noise input randomly selected from a uniform distribution, chosen from the interval [-0.2, 0.2].

Four experiments were simulated with the SVD task. The first experiment examined the learning and performance of the SVD task under high uniform DRIVE inputs. This experiment involved discriminating a rewarded from an unrewarded stimulus. The second experiment

examined the change in saccadic reaction times when the rewarded stimulus was paired with a food reward that had been devalued by FSS (for a discussion of the dynamics of SVD task performance, see Supplementary Notes 3). In order to simulate FSS, DRIVE inputs and HAB transmitter gates associated with Food 1 were reduced in a food-specific fashion. The third variant of this task involved measuring the differences in saccadic reaction time when the target of a discrimination earned a large reward versus when the target of a discrimination earned a small reward. The magnitude of the GUS input (a value of 1 or 0.5) determined large and small rewards.

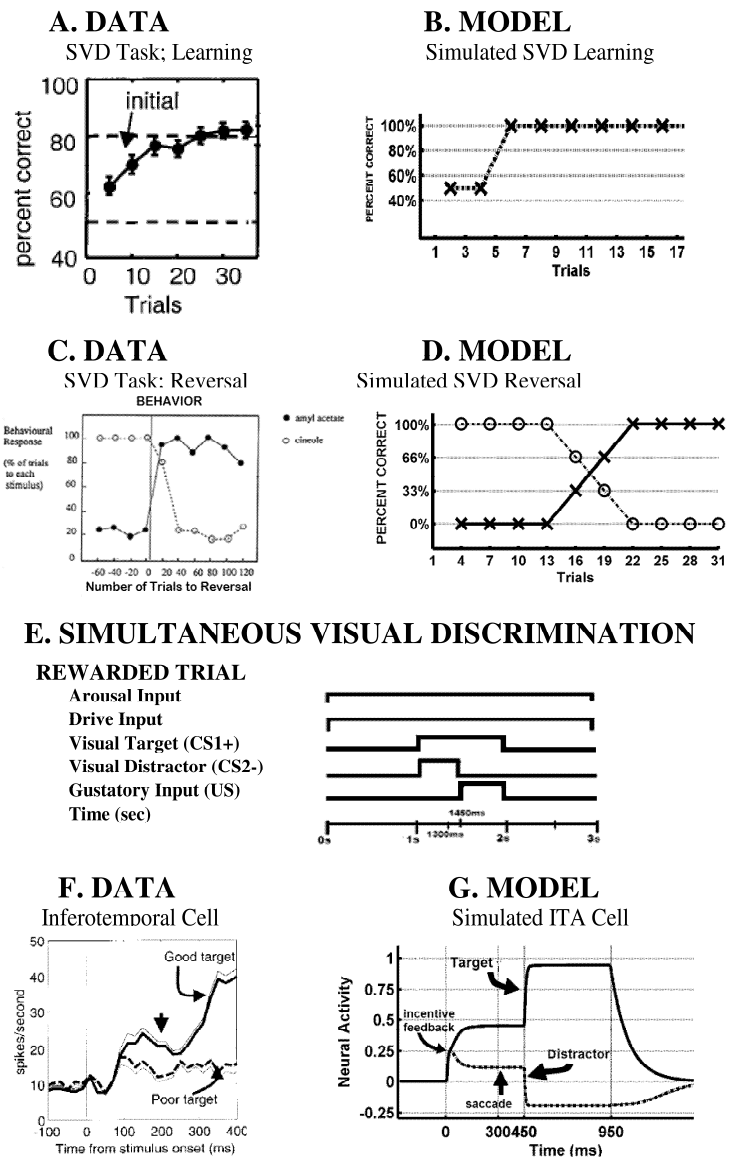

Figure 5: SVD Task training and cell responses. (A) Learning and acquisition of SVD task (reprinted with permission from Jagadeesh et al. 2001). Each point represents the percentage of correct responses in a block of 5 trials. (B) Simulated learning and acquisition of SVD task. Each point represents the percentage of correct responses in a block of 3 trials. (C) Reversal of SVD task (reprinted with permission from Rolls et al. 1996). Each point represents the percentage of correct saccades in a block of 20 trials. (D) Simulated reversal of SVD task. Each point represents the percentage of correct saccades in a 3 trial block. (E) SVD timing (Jagadeesh et al., 2001). Two visual stimuli are presented simultaneously. When the rewarded stimulus (target) is selected, the unrewarded stimulus (distractor) terminates The target stimulus remains on for 500ms while a gustatory reward is presented. No reward is given on error trials. (F) Response of inferotemporal cells during the SVD task (reprinted with permission from Jagadeesh et al., 2001). Solid line indicates the activity of an IT_a cell to its favored stimulus is enhanced when it is the target of an SVD problem. Dashed line indicates the activity of an IT_a cell is suppressed when its favored visual stimulus is the distractor of an SVD problem. (G) Model IT_a cell activity during the SVD task may be enhanced or suppressed depending on whether the visual stimulus to which the IT_a cell selectively responds is associated with reward or nonreward. These attentional enhancements are mediated by incentive feedback from the ORB_l. After the distractor terminates, contrast normalization boosts the IT_a cell response to the remaining stimulus.

The fourth version of this task examined how DRIVE inputs alter decision-making. In the previously described SVD task, a choice is made between a rewarded and an unrewarded stimulus. In the SVD-FSS task, however, a choice is made between two differently rewarded stimuli. Most often, the stimulus associated with the most preferred reward is selected in the task. Prior to testing these stimulus preferences, each stimulus (CS1 or CS2) is trained in parallel using a distinct reward (US1 or US2). This training establishes a strong association between specific stimuli and rewards (CS1-US1 vs. CS2-US2). The SVD-FSS task is used to examine how drive alters decision-making by assaying how stimulus preferences change before and after food-specific satiety. Stimulus preferences under high hunger conditions are simulated using high DRIVE inputs. Low DRIVE inputs are used to simulate stimulus preferences after the induction of a food specific satiety. This shift from high to low DRIVE levels directly alters stimulus preferences, even when no rewards or additional training occurs.

This automatic shift in preferences relies on competing stimuli activating different outcome-specific value cells in the AMYG so that decision-making in the ORB_l is informed by the current motivational value of different expected outcomes. This outcome-specific information is elicited when stimuli activate conditioned reinforcer learned associations from the IT_a to the AMYG, incentive motivational learned associations from the AMYG to the ORB_l, value category learned associations from the LH to the AMYG, and appetitive priming associations from the AMYG to the LH. Taken together, these several types of learning and their interactions explicate earlier concepts of stimulus-outcome associations.

These learned associations ensure that stimulus value automatically shifts to reflect the current value of predicted rewards, given the current needs of the animal and feedback interactions between the AMYG and LH (see Supplementary Notes 3).

The protocol for the second-order conditioning (SOC) task combined elements of SVD and CS tasks. In particular, the conditioned reinforcer (first-order CS) was trained using the CS task protocol (delay conditioning), while the second-order CS was conditioned using a protocol similar to the SVD task (overlap conditioning). Prior to initiating second-order conditioning, the conditioned reinforcer was trained for fifteen trials using the CS task protocol. After the conditioned reinforcer was trained, second-order conditioning occurred. During SOC trials, the second-order CS was paired with a conditioned reinforcer (first-order CS) using an overlap conditioning paradigm.

In particular, the second-order visual stimulus was presented for 500ms followed by the first order stimulus for 500ms with 100ms overlap. Fifteen trials were used for training. The first-order CS was retrained every other trial. These experiments were performed under uniform high DRIVE inputs. A delay conditioning paradigm was not used in the SOC task paradigm because the capacity of the first-order CS to drive outcome-specific conditioning (conditioned reinforcer learning) depended greatly on DRIVE inputs and the level of AMYG activation during training. Conditioned reinforcer learning is much stronger when a CS is paired with a US than during second-order conditioning, because a first-order CS samples a much stronger US-related signal, driven by GUS inputs, which strongly activate the LH and AMYG.

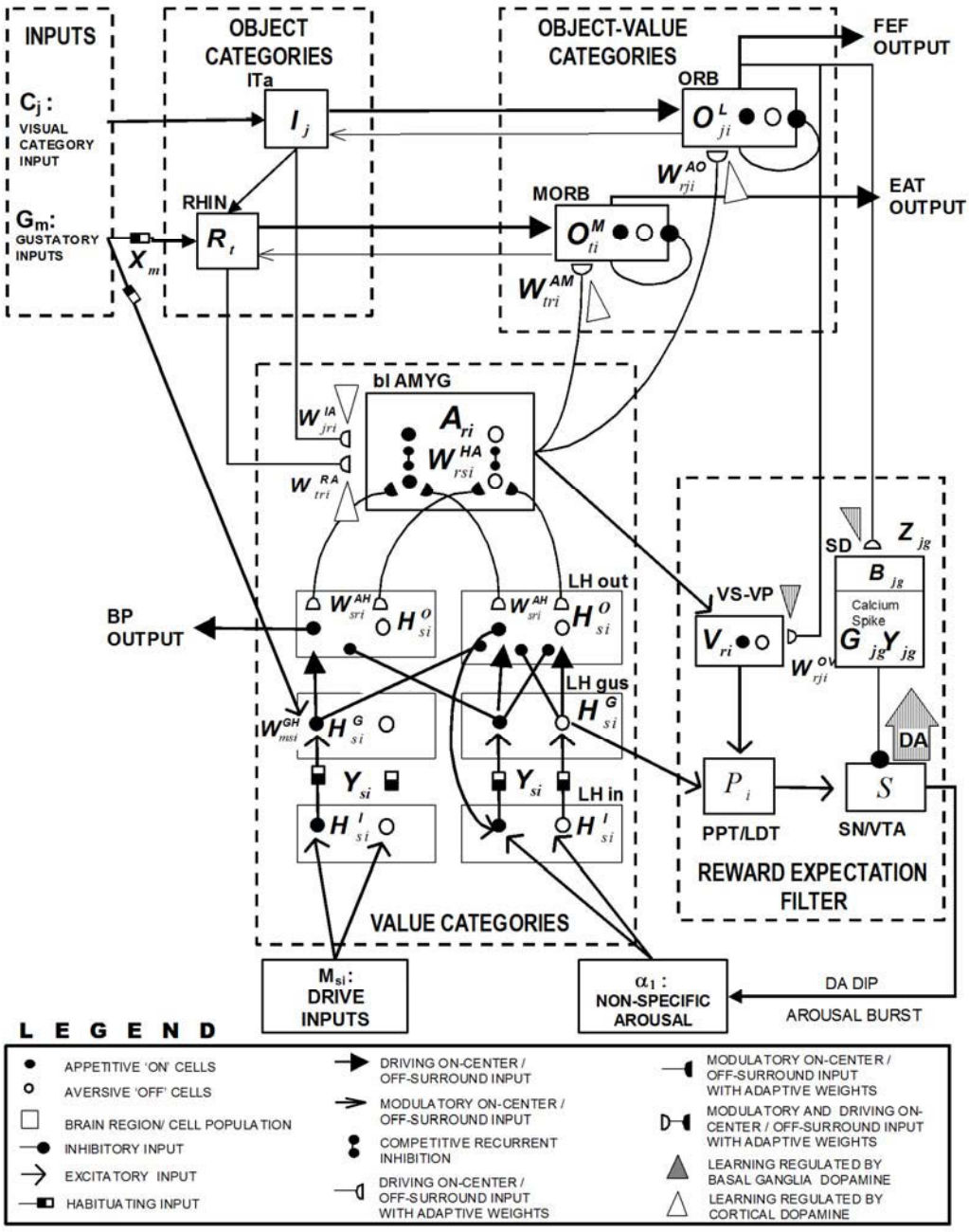

Figure 6: Model detail with equation variables. Distinct cell types are represented with different labeled compartments. Cells may or may not show a selective response to affective information of different valences. Cells which selectively respond to appetitively valenced information are indicated by filled circles. Cells which selectively respond to aversive affective information are indicated by open circles. Activation is transmitted between cells along specific pathways. Pathways are indicated by edges with arrowheads (fixed excitatory connection), semicircles (learned excitatory connection), or filled circles (fixed inhibitory connection). Filled arrowheads carry driving excitatory inputs. Open arrowheads carry excitatory signals that modulate or multiply driving inputs. Similarly, filled semicircles carry adaptively gated driving inputs while open semicircles carry adaptively gated signals that modulate driving inputs. Half-filled rectangle: Pathways which show activity driven habituation. Weights ('W') have a pathway specific superscript. Lateral hypothalamic cells are expanded from Figure 1 to describe three classes of cells: drive receptive (LH in cells), gustatory receptive (LH gus), and output cells (LH out). For variable names, subscript and superscript definitions, and other details see Supplementary Equation Appendix.

The sensitivity of second-order conditioning to DRIVE input levels and training protocol is consistent with the observation that some researchers have had difficulties conditioning outcome-specific associations with second-order conditioned stimuli (Hall, 2001). In addition to simulations where the SOC task was trained after AMYG and ORB lesions ('AX' and 'OX' in the figures), simulations were performed where the AMYG was lesioned only after the SOC task was trained. For this 'pretrained' AMYG lesion simulation ('pre-AX' in the figures), the model was trained with twenty trials of the CS task before the amygdala was lesioned.

Model anatomy

The MOTIVATOR model uses the same system architecture (Figure 1) to perform all three tasks, with elaborations provided as necessary to account for the additional competencies needed to solve each more difficult task. The model incorporates four functional classes of brain regions: (1) Sensory Categories register visual (inferotemporal, IT_a) or gustatory inputs and (rhinal, RHIN) inputs; (2) Drive-Value Categories calculate the value of specific food rewards using a combination of drive and affective information (amygdala, AMYG; and lateral hypothalamus, LH); (3) Object-Value Categories resolve the expected value of competing stimuli and rewards (lateral orbitofrontal cortex, ORB_l; medial orbitofrontal cortex, ORB_m); and a (4) Reward Expectation Filter detects the unexpected occurrence or omission of rewards and punishments (basal ganglia, BG).

The model architecture represents a synthesis and further development of four previously described model circuits; namely, Cognitive-Emotional-Motor, or CogEM, circuits; Adaptive Resonance Theory, or ART, circuits; recurrent gated dipole opponent processing circuits; and basal ganglia adaptively timed learning and matching circuits from the TElencephalic Laminar Objective Selector, or TELOS, model. Each of these circuit elements models different aspects of sensory, cognitive, emotional, motivational, and motor processing.

CogEM model. The CogEM model (Grossberg, 1971) forms the core of the MOTIVATOR model. The CogEM model clarifies how sensory representations (e.g., inferotemporal cortex, IT_a), drive representations (e.g., amygdala, AMYG; and lateral hypothalamus, LH), and object-value representations (e.g., orbitofrontal cortex, ORB_l) interact via conditioned reinforcer, incentive motivational, and motor learning pathways (Figure 1). In particular, sensory representations compete for storage in short term memory. Drive representations are activated by conditioned or unconditioned reinforcers. Object-value representations are activated when they receive inputs simultaneously from sensory representations and drive representations. The inputs from the drive representations provide incentive motivation to fire the corresponding sensorily-activated object-value representations. When object-value representations are sufficiently activated, they can elicit outputs to motor representations where responses to targets are elaborated.

These components are linked by pathways in which at least three types of learning occur: *Conditioned reinforcer learning* takes place in the pathways from sensory representations to drive representations. *Incentive motivational learning* takes place in the pathways from drive representations to object-value representations. *Motor learning* takes place in the output pathways that are activated by the object-value representations.

Thus, in response to visual cues, object-selective sensory representations in the inferotemporal cortex learn to activate drive representations in the amygdala via learned conditioned reinforcer pathways. Activated drive representations can, in turn, activate the prefrontal cortex via learned incentive motivational pathways. Motivationally salient sensory representations can hereby provide inputs directly to prefrontal object-value representations, and

indirectly via the two-step learned conditioned reinforcer and incentive motivational pathway through the drive representations. The incentive input determines how vigorously the object-value representation is activated (Schoenbaum et al., 2003). The most active object-value representations can select, and focus attention upon, motivationally consistent sensory representations via positive feedback to the sensory representations combined with competition among the sensory representations. The motivationally most salient sensory representations can hereby attentionally block irrelevant sensory cues. At the same time, active object-value representations can read-out commands to control motivationally relevant actions. These properties of the CogEM model have been used to explain and simulate many data concerning conditioning and its modulation by motivated attention (Grossberg, 1971, 1975, 1982, 1984, 2000; Grossberg and Levine, 1987; Grossberg and Schmajuk, 1987; Grossberg and Seidman, 2006).

The MOTIVATOR model extends the sensory representations to include taste representations (rhinal cortex, RHIN) and the corresponding object-value representations (medial orbitofrontal cortex, ORB_m) circuits. The MOTIVATOR model hereby proposes parallel CogEM networks to process visual and gustatory information (cf., Barbas, 1995). Gustatory and taste reward information is processed via a CogEM circuit linking the gustatory cortex, rhinal cortex, amygdala, and orbitofrontal cortex (Dunn and Everitt, 1988; Baylis and Gaffan, 1991; Murray et al., 1996; Parker and Gaffan, 1998). Visual discrimination and conditioned reinforcer-related processing occur via a parallel CogEM circuit linking the inferotemporal cortex, amygdala, and orbitofrontal cortex (Malkova et al., 1997; Baxter et al., 2000; Easton and Gaffan, 2000). Supplementary Notes 4 describe how the CogEM model is implemented in the current model.

ART model and drive-value categories. The ART model (Carpenter and Grossberg, 1991; Grossberg, 1980, 1999) is used to clarify how distributed patterns of appetitive signals in the LH learn to selectively activate drive-value categories in the AMYG, and how activated AMYG categories can send learned top-down signals to the LH to prime expected patterns of appetitive signals there. These reciprocal interactions between the AMYG and LH calculate the motivational or drive value of conditioned and unconditioned reinforcers and explain how satiety devalues reinforcers in a food-specific fashion. Combining these CogEM and ART properties allows a CS to elicit an autonomic response by activating the AMYG via conditioned reinforcer pathways, which in turn activates autonomic responses via the LH.

The MOTIVATOR model explains how outcome-specific drive and incentive information, such as the affective and drive properties of unconditioned stimuli, can alter the salience and vigor of conditioned stimuli and responses (Hall, 2001; Rescorla, 1991). The properties of US-activated drive-value category cells in the amygdala play an important role in the model's explanations of how this happens. The hypothesis that the amygdala derives many of its reinforcing and motivating properties by learning such drive-value categories is a new feature of the model. In particular, such amygdala categories interact with taste-drive feature cells in the lateral hypothalamus to calculate the value of food rewards given the current needs of the animal.

These taste-value feature cells are a specific kind of object-value representation. Taste-drive feature cells are cells that respond to one metabolic input and its correlated taste; for example, a cell that senses glucose and responds to sweet tastes. US drive-value category cells are learned in the amygdala during the US consumption. When a US is consumed, gustatory inputs activate a distributed pattern of activity in taste-drive feature cells in the lateral hypothalamus. This pattern of activation is associated with the metabolic profile of the US. Adaptively weighted connections from taste-drive feature cells activate amygdala drive-value

category cells (Figure 1). As a result of a competitive learning process, these adaptive weights form a compressed code that allows a particular drive-value category cell, or cell population, to selectively respond to and recognize a reward-specific pattern of taste-drive feature cells. At the same time, these US-activated drive-value category cells learn via adaptively weighted reciprocal top-down connections to reinstate the activity pattern across the taste-drive feature cells that is associated with US consumption.

Once such a drive-value amygdala category cell is learned, it calculates the value of a US by summing the activation of US-related taste-drive hypothalamic feature cells. Owing to the recurrent connections between the drive-value categories and the taste-drive feature cells, this summation is nonlinear, but the bias that is introduced respects empirical observations of valuation (Kahneman and Tversky, 1979). In particular, during consumption, US value is not a simple summation of metabolic and taste information, because taste-drive cells multiply taste and drive information together (Grossberg, 1984), resulting in a US value that is instead comparable to the sum of the expected values of each taste. When testing the value of a prospective outcome, activating a drive-value category cell determines US value by top-down activation of US-related taste-drive feature cells. These top-down signals substitute for gustatory inputs. Each top-down input is individually multiplied by current drive levels, resulting in feedback to the drive-value category cell that reflects the sum of expected values that corresponds to that US. When multiple US value category cells simultaneously sample the value of prospective outcomes, there is strong competition between them. This competition is weaker than winner-take-all, resulting in a softmax analog activation of the strongest competing prospects.

Various data support the model hypothesis that US drive-value category cells are found in the amygdala and taste-drive feature cells are found in the lateral hypothalamus. Multimodal amygdala cells that are food selective and respond in proportion to the value of a food reward have been extensively studied in the primate and rodent (Nishijo et al., 1988; Toyomitsu et al., 2002). Lateral hypothalamic cells are considered to be the site of taste-drive feature cells that sense the levels of different metabolites and respond to correlated tastes and cues. For example, glucose-sensitive cells in the lateral hypothalamus measure the drive to consume glucose: They increase their activity in response to decreases in blood glucose levels (Sikdar and Oomura, 1985), increase their responses when a sweet taste is presented (Karadi et al., 1992), and increase their responses when a visual cue that predicts a sweet taste is presented (Ono et al., 1986).

Recurrent gated dipole. The recurrent gated dipole module describes how opponent processing of appetitive and aversive affective signals in the AMYG and LH are used to regulate conditioned reinforcer and incentive motivational learning and performance (Grossberg, 1972, 1975, 1982, 1984, 2000; Grossberg and Schmajuk, 1987; Grossberg and Seidman, 2006). Such circuits are incorporated into the LH and AMYG of Figure 1 to show how motivationally opponent pathways can habituate in an activity-dependent manner. Such habituation sets for stage for enabling both rapid changes in phasic reinforcing inputs and unexpected events to cause antagonistic rebounds in affective valence in the LH, thereby resetting the corresponding drive-value categories in the AMYG.

A motivational gated dipole circuit incorporates five components: (1) ON and OFF channels that receive phasic appetitive and aversive inputs, respectively; (2) a nonspecific arousal signal to both the ON and OFF channels that sets the circuit's adaptation level and provides the internal activation that energizes antagonistic rebounds; (2) habituating transmitter gates in both channels that slowly adapt to the total phasic-plus-tonic input to each channel, and

whose imbalance determines which of the ON or OFF channels generates outputs at any time; (4) competition between the transmitter-gated signals in the ON and OFF channels to ensure that just one ON or OFF output is active at a time; and (5) rectification of the net activities after competition to generate positive output signals from the circuit. For a discussion of its derivation and behavioral applications, see Supplementary Notes 5.

In the MOTIVATOR model, the gated dipole circuit models the activity of lateral hypothalamic *opposite cells* and *specific cells* (Ono et al., 1986). Opposite cells are proposed to be LH output cells, and specific cells are LH input and LH gustatory receiving cells (see Figure 5a). The lateral hypothalamus is the primary model region where hunger and satiety inputs are segregated into behaviorally relevant appetitive and aversive signals (Swanson, 2000; Bernardis and Bellinger, 1996). The MOTIVATOR model also incorporates recurrent or feedback connection within the gated dipole circuit (cf., Grossberg, 1982; Grossberg and Schmajuk, 1987). These recurrent connections enable the dipole to maintain a stable motivational choice despite small input fluctuations, to support secondary excitatory and inhibitory conditioning, and to enable amygdala-based inputs to drive adaptation of hypothalamic taste-drive feature detectors.

TELOS model and its basal ganglia circuit. The MOTIVATOR model incorporates basal ganglia circuits to describe how dopamine signals from the substantia nigra are activated in response to rewards and nonrewards that are unexpected in terms of their size, timing, or both. These mismatch-activated dopamine signals are broadcast throughout the brain to learn new cognitive and motor plans (Schultz, 1998, 2007; Fiorello et al., 2003). These predictive errors are signaled by dopamine bursts and dips that modulate learning and extinction, respectively. These basal ganglia circuits are part of the larger TELOS model of Brown et al. (1999, 2004) which clarifies the general problem of how the brain learns to balance between reactive and planned behaviors. The basal ganglia and frontal cortex together allow animals to learn planned behaviors that acquire rewards when prepotent reactive behaviors are insufficient. The TELOS model was developed to explain how laminar circuitry of the frontal cortex interacts with the basal ganglia, thalamus, superior colliculus, and inferotemporal and parietal cortices to learn and perform reactive and planned eye movements. The model incrementally learned five tasks that monkeys have been trained to perform. After learning, model dynamics quantitatively simulated the neurophysiologically recorded dynamics of seventeen different identified cell types (Hanes et al., 1998; Hikosaka & Wurtz, 1989; Kalaska & Crammond, 1995; Munoz & Wurtz, 1993, 1995; Schall, 1991; Schall et al., 1995a, b; Schlag-Rey & Schlag, 1984; Turner & Anderson, 1997; Wichmann et al., 1994) and predicted distinct functional roles for all of them.

The MOTIVATOR model does not incorporate the entirety of TELOS, but only the basal ganglia circuit that learns to detect the occurrence of unexpected rewards or nonrewards (Brown et al., 1999, 2004). This basal ganglia circuit (Figure 1) includes cells from the ventral striatum, ventral pallidum, pedunculopontine nucleus (PPTN), striosomal striatum cells, the orbitofrontal cortex, lateral hypothalamus, and dopaminergic midbrain (VTA/SNc). Unexpected primary rewards elicit dopamine bursts via an excitatory pathway from the lateral hypothalamus and PPTN to the VTA/SNc. Conditioned reinforcer inputs from the amygdala or orbitofrontal cortex can also trigger a dopamine burst in the VTA/SNc via a net excitatory input from the ventral striatum and ventral pallidum (Figure 1).

Within the basal ganglia, these dopamine bursts and dips serve to train striosomal striatal cells to generate a burst of inhibitory activity at the expected time of reward. Calcium dynamics control the timing of this burst (also see Fiala et al., 1996). When this inhibitory signal reaches

the SNc/VTA, it can cause a dip in dopamine activity if the expected reward is omitted. If the reward is presented as expected, the inhibitory signal generated by striosomal striatal cells cancels the expected dopamine burst, resulting in no net activation of dopamine cells. If a primary or conditioned reward occurs at an unexpected time, the inhibitory signal is not present to prevent the burst. Likewise, if the reward occurs with an unexpectedly large (small) amplitude, it can partially overcome the amplitude of the inhibitory signal, leading to a burst (dip), even if they occur at the same time. Such dopamine bursts and dopamine dips drive learning and extinction by being broadcast as Now Print modulatory signals to wide regions of the brain. When the full TELOS model is joined to MOTIVATOR, these dopamine signals are sufficient to underlie the training of the SVD task via habit learning mechanisms, just as TELOS can learn other types of rewarded sensory-motor tasks.

In the MOTIVATOR model, dopamine signals also play a critical role gating conditioned reinforcer and incentive motivational learning. In particular, the model proposes that dopamine signals from the basal ganglia interact with gated dipole mechanisms in the lateral hypothalamus. For example, on extinction trials, a dopamine dip occurs when an expected reward is omitted. This dopamine dip can elicit a burst in arousal inputs to the lateral hypothalamus, possibly via the central amygdala as transient inactivation of this nucleus leads to the powerful nonspecific activation of LH cells (Fukuda and Ono, 1987; Nakamura, et al. 1987). This arousal burst saturates opponent channels in the LH, terminating activity in lateral hypothalamic output cells. The termination of AMYG activity closely follows the termination of LH activity, speeding extinction of conditioned reinforcer connections. This temporary inactivation protects drive-value categories in the amygdala from being extinguished along with stimulus-outcome associations between the IT_a, ORB_l, and AMYG. In the reverse direction, the AMYG and LH often generate appetitive rebounds following rapid changes in the amplitude of reinforcing inputs. This rebound activation can activate the PPTN and trigger a dopamine burst.

The model, as summarized in Figure 1, enables the following types of interactions: In the US task, food rewards are recognized by the RHIN and evaluated with respect to current needs in the AMYG. US identity and US drive-value information are fused in the ORB_m to calculate the expected value of the US and drive consumption behavior. Autonomic responses to the US, in the form of changes in systolic blood pressure, are generated during consumption via signals from the LH. US consumption activates LH via taste pathways, and AMYG via RHIN pathways (Figure 1). These LH and AMYG activations can, in turn, cause reinforcing dopamine bursts from the basal ganglia. The basal ganglia can also influence, indeed reset, the current state of the LH and AMYG, as noted below.

In the CS task, a visual stimulus CS is recognized by cells in IT_a. IT_a, in turn, learns to activate the AMYG via conditioned reinforcer pathways, as a result of conditioning trials during which the CS is paired with the US (Figure 1). AMYG cells can then respond to the CS in proportion to the value of the expected US. As training of the conditioned reinforcer pathway from IT_a to AMYG takes place, the AMYG also learns to activate the ORB_l via incentive motivational learning. The ORB_l receives prospective US value information via IT_a-activated incentive motivational pathway from AMYG, and combines it with CS identity information directly from IT_a. Together these inputs enable ORB_l cells to calculate the expected value of the CS. In other words, the combination of direct IT_a activation and indirect activation via AMYG endows ORB_l cells with object-value properties. ORB_l also has feedback connections with IT_a. When a conditioned stimulus is trained, a positive feedback loop is learned that enables ORB_l to attentionally select behaviorally relevant stimuli in IT_a and to suppress others, as during

attentional blocking (Grossberg and Levine 1987; Kamin, 1969; Pavlov, 1927). Activated ORB_l cells can also elicit approach responses.

When an expected reward is omitted following CS presentation, dopamine dip signals are generated in the basal ganglia, which cause a burst of nonspecific arousal that is felt in multiple brain areas. When this arousal burst reaches the LH, its gated dipole circuits respond with an antagonistic rebound of activation that terminates activity in currently active LH cells and transiently activates LH cells that were previously suppressed by opponent inhibition (Grossberg, 1972, 1982, 1984; Nakamura and Ono, 1986; see Supplementary Notes 5). As noted above, the model predicts that these antagonistic rebounds in the LH also shut off the corresponding active drive-value category cells in the AMYG. This is consistent with the observation that cue- and reward-activated AMYG cells are inhibited when expected rewards are omitted (Belova, et al. 2007). This AMYG inactivation speeds the extinction of conditioned reinforcer learning from IT_a to AMYG, thereby ensuring that changes in cue preference can occur quickly. As a result, formerly predictive cues become emotionally irrelevant. The rapid inactivation of AMYG drive-value category cells also leads to the relative sparing of incentive motivational learning from AMYG to ORB_l, and of the learned connections between the AMYG and LH, whereby the LH can selectively activate AMYG drive-value categories, and the AMYG categories can prime LH appetitive patterns. Thus the AMYG can preserve its drive-value category properties even while the CS extinguishes.

In the SVD task, two visual cues are presented simultaneously and recognized by different IT_a cells. The stimulus associated with the more valuable reward activates a stronger positive feedback loop from the AMYG to the ORB_l and back to IT_a, just as occurs during an attentional blocking experiment. Projections from the ORB_l to the FEF use the ORB_l's expected value information to influence the probability and latency of saccades.

Simulation Notes and Equations. The model was simulated as a system of differential equations using MATLAB and a fourth-order Runge-Kutta numerical integration routine. Neural populations were simulated using short term memory equations (STM). Synaptic efficacy is altered by transmitter habituation and learning. Habituating sensory gates were modeled with medium term memory equations (MTM). Learning relies on adaptive synaptic weights that were modeled with long term memory equations (LTM). There were four types of inputs to the system: Visual (VIS) inputs C_j, gustatory (GUS) inputs G_m, drive or metabolic inputs M_s, and arousal inputs, α_1 and α_2. The subscript *j* indexes different visual stimuli, C_j; the subscript *m* indexes different tastes, G_m, including sweet, salty, savory (umami), and fatty; the subscript *s* indexes different metabolic drives that are correlated to taste, M_s, including sugar, salt, protein, and fat. Arousal inputs include an input α_1 to the lateral hypothalamus (see Supplementary Notes 5). In addition, the PPTN receives an arousal input α_2 that elevates baseline firing rate, rendering the output of PPTN cells sensitive to inhibitory inputs from the VS-VP. Model outputs include saccadic eye movements elicited by frontal eye fields (FEF), feeding responses initiated by the cortical masticatory area (CMA), systolic blood pressure signals (BP) derived from LH_out cell activity (Figure 5a), and dopamine signals from SNc/VTA (see Figures 1, 2, and 5).

The STM activity of neurons is derived from the membrane equation (Grossberg, 1973; Hodgkin and Huxley, 1952):

$$C_m \frac{dV(t)}{dt} = (R_{leak} - V(t))g_{leak} + (R_{excite} - V(t))g_{excite} + (R_{inhibit} - V(t))g_{inhibit} . \quad (1)$$

In (1), $V(t)$ is compartment membrane potential, C_m is the membrane capacitance constant, $g_{excite}(t)$ and $g_{inhibit}(t)$ are conductances for excitatory and inhibitory current inputs, and R_{excite} and $R_{inhibit}$ are reversal potentials for these current inputs. Terms g_{leak} and R_{leak} are the leakage conductance and reversal potential of leaked ions. Reversal potentials are rescaled in the simulated equations such that $R_{excite} \equiv 1$ and $R_{leak} \equiv 0$. The inhibitory reversal potential was rescaled in a cell-specific fashion taking values of 0, -0.2, or –1. Simulated equations included shunting equations such as (1):

$$\tfrac{1}{\tau}\frac{d}{dt}V_i = -V_i + (1-V_i)E_i - (C+V_i)I_i \ ; \tag{2}$$

and 'cortical-type' shunting equations:

$$\tfrac{1}{\tau}\dot{V}_i = -V_i + (1-V_i)\left(D_i\left(1+M_i\right)\right) - (C+V_i)\left(\sum_{k\neq i} D_k + \sum_{k\neq i} M_k\right); \tag{3}$$

and additive approximations to shunting equations:

$$\tfrac{1}{\tau}\frac{d}{dt}V_i = -V_i + E_i - I_i. \tag{4}$$

Variable V_i is the rescaled activity of each neural cell population with ($V_i \in$ [1, -C], where $C \in$ {1, 0.2, 0}). Term $-V_i$ represents the decay of neural activity toward the leakage reversal potential, E_i denotes excitatory inputs, I_i denotes inhibitory inputs, and τ defines the decay rate. 'Cortical-type' equations, inputs have an on-center, off-surround anatomy where on-center inputs are indicated with a subscript *i*, and off-surround inputs are indicated by summation across the dummy variable $k \neq i$. Excitatory inputs are either driving, D_i, or modulatory, M_i, on-center inputs. Inhibitory inputs $\left(\sum_{k\neq i} D_k + \sum_{k\neq i} M_k\right)$ are all driving off-surround inputs. This arrangement enables activities to contrast normalize their inputs patterns.

Lateral hypothalamic cells were simulated using a mixture of additive (LH input cells, LH gustatory cells) and shunting equations (LH output cells). RHIN, IT_a, ORB_l, and ORB_m cells were simulated using cortical-type shunting equations. The AMYG was also simulated using cortical-type shunting equations, but with a recurrent term that allowed for competitive choices (for parameters and additional details see Supplementary Equation Appendix). The competitive dynamics in the AMYG allow AMYG cells to learn to selectively respond to specific patterns of LH cell activation. Feedback projections from the AMYG to the LH help stabilize these learned patterns and enable the AMYG to use current needs to estimate the value of prospective (see Supplementary Notes 1-4). The systolic blood pressure and FEF were simulated using additive equations. In the basal ganglia, the VS, SNc/VTA, PPTN, and striosomal striatum were simulated using shunting equations.

Medium term memory (MTM) equations describe how recent use of synapses affects the gain of signals transmitted through these synapses from one brain region to another. To capture these habituation (inactivation, depressing) effects, MTM equations describe fluctuations in the accumulation and depletion of a chemical transmitter G:

$$\dot{G} = \left(1-G\right) - G\left[V\right]^{+}. \tag{5}$$

(Grossberg, 1972, 1980). In (5), G is the available transmitter, scaled between [0, 1]; term $\left(1-G\right)$ describes transmitter recovery; term V_i is the signal function of the transmitting neuron;

and $G[V]^+$ is the activity-gated inactivation rate of the transmitter. GUS inputs were associated with a habituating term that modeled taste-specific habituation. LH input cells also had a habituating gate that adapted to DRIVE and AROUSAL inputs.

Long term memory (LTM) is formed by learned lasting changes in the conductive efficacy of synapses (Brown et al., 1990). LTM variables function as weights that gate signals transmitted between different brain regions. LTM learning equations describe how neural activity alters these weights. The model employs two basic LTM equations: (1) activity-gated steepest-descent learning; and (2) dopamine-gated steepest-descent learning. The former equations involve *outstar* equations where learning is gated by a presynaptic signal and synaptic weights learn about postsynaptic activity and *instar* equations where learning is gated by a postsynaptic signal and synaptic weights learn about presynaptic signals (Grossberg, 1968, 1972); e.g.,

$$\varepsilon \dot{W}_{jk} = S_j \left(T_k - W_{jk} \right), \tag{6}$$

where W_{jk} represents the LTM weight, S_k represents the postsynaptic signal, and T_j represents the presynaptic signal. These equations were used to model adaptive connections from the AMYG to LH and from the LH to the AMYG.

For dopamine-gated LTM equations, dopamine activity doubly-gates learning in *instar* and *outstar* equations. In these equations, dopamine dips speed weight decay of appetitive stimuli and dopamine spikes speed appetitive learning; e.g.,

$$\varepsilon \dot{W}_{jk} = S_k \left[\left(A + D_1 \right) \left(T_j - W_{jk} \right) - \left(A + D_2 \right) W_{jk} \right], \tag{7}$$

where D_1 represents a dopamine spike and D_2 a dopamine dip. These equations were used to model adaptive weights to and from the AMYG (from the IT_a to the AMYG, from the RHIN to the AMYG, from the AMYG to the ORB_l, from the AMYG to the ORB_m), and adaptive weights from the ORB_l to ventral striatum. For parameters and additional details on all equations, see the Supplementary Equation Appendix.

Lesion Recovery Equations

Simulated amygdala lesions were implemented by setting all AMYG parameters to zero (see Supplementary Equation Appendix). Eliminating AMYG activity strongly suppresses ORB_l cell activity. To simulate recovery processes (Leonard, et al. 1996), parameters were changed, and the gain of IT_a inputs to the ORB_l was increased. Prior to the AMYG lesion, the ORB_l equation is:

$$\tfrac{1}{50} \dot{O}^L_{ji} = -O^L_{ji} + (1 - O^L_{ji}) \left(0.1 \left[I_j \right]^+ \left(1 + 160 \sum_r W^{AO}_{jri} \left[A_{ri} \right]^+ \right) \right) - (O^L_{ji}) \left(2 \sum_{k \neq j} \sum_r W^{AO}_{kri} \left[A_{ri} \right]^+ + 0.2 \sum_{k \neq j} \left[I_k \right]^+ + 50 \sum_{l \neq i} \left[O^L_{jl} \right]^+ \right). \tag{8}$$

See Figure 5a for variable names and the Supplementary Equation Appendix for discussion of equation terms. Post-lesion, the ORB_l equation becomes:

$$\tfrac{1}{50} \dot{O}^L_{ji} = -O^L_{ji} + (1 - O^L_{ji}) \left(10 \left[I_j \right]^+ \right) - (O^L_{ji}) \left(\left(0.2 \sum_{k \neq j} \left[I_k \right]^+ \right) + \left(50 \sum_{l \neq i} \left[O^L_{jl} \right]^+ \right) \right). \tag{9}$$

This parameter change is congruent with the increase in sensory responsiveness and decrease in motivational sensitivity observed in ORB_l cells following AMYG lesions (Schoenbaum, et al. 2003). The parameter change also ensures ORB_l responses remain strong enough to drive VS and SD cells, and to ensure that dopamine cells in the SNc/VTA continue to be able to detect unexpected reward or nonreward. Without ORB_l inputs to SD cells, the delivery time of expected rewards cannot be anticipated (see Figure 1).

Simulated ORB lesions were implemented by setting ORB_l and ORB_m equations to 0.

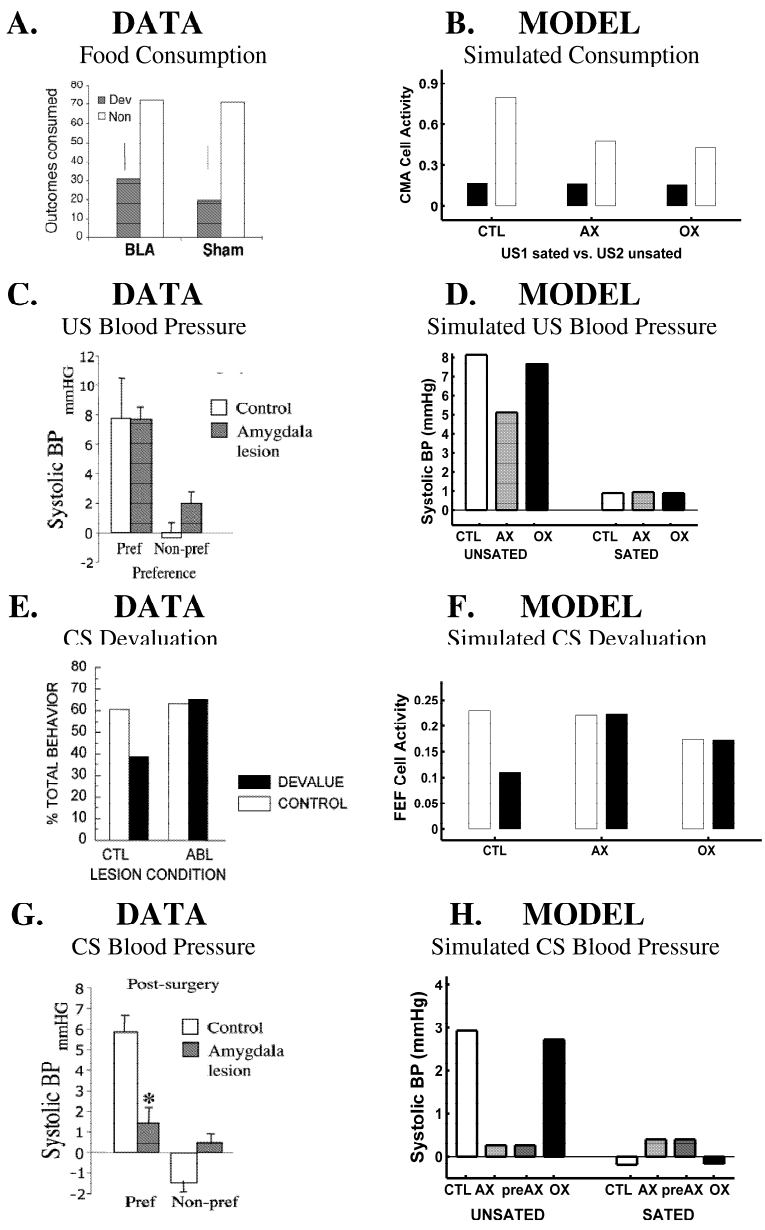

Figure 7: Revaluation of conditioned and unconditioned responses. (A) Food-specific satiety (FSS) reduces food consumption in normal and amygdala-lesioned animals (BLA; reprinted with permission from Corbit and Balleine, 2005). Bars indicate the amount of food consumed before (white) and after FSS (gray). (B) Model Simulations show suppressed food consumption after US devaluation by FSS when the model is intact (CTL) and when the AMYG (AX) or ORB_l (OX) is lesioned. Bars reflect average CMA cell activity across the two second US presentation before (white) and after FSS (black). (C) Consumption of a valued food is associated with an increase in systolic blood pressure for both intact (white) and amygdala-lesioned animals (black; reprinted with permission from Braesicke et al., 2005). Bars indicate increase in blood pressure relative to resting systolic blood pressure. (D) Model predicts systolic BP is elevated during consumption of unsated foods when the model is intact (CTL) and even when the AMYG or ORB_l is lesioned (AX and OX). This effect is not seen when sated food rewards are consumed. Bars reflect difference between average simulated resting systolic BP and systolic blood pressure during the US presentation. (E) Sham-lesioned animals (white bars) automatically reduce the frequency of Pavlovian responses when the US associated with a CS is devalued by FSS (reprinted with permission from Hatfield et al., 1996). Amygdala lesions block this automatic revaluation of Pavlovian responding (black bars). (F) Model simulations show that devaluing the US automatically reduces Pavlovian responding for an associated CS when the model is intact (CTL) but not when the model AMYG (AX) or ORB_l (OX) is lesioned. This impairment in automatic revaluation of Pavlovian responding is also seen when the CS is trained prior to model AMYG being lesioned (preAX). Bars indicate average FEF activity during CS presentation. (G) Sight of a desired food reward elevates systolic blood pressure for control (white bar) but not amygdala-lesioned animals (gray bar; reprinted with permission from Braesicke et al., 2005). Bars reflect difference between average CS-elicited systolic blood pressure and average resting systolic blood pressure. (H) Model simulations show that a CS associated with an unsated food reward evokes an elevation in systolic blood pressure for the intact and ORB_l -lesioned variants of the model (CTL and OX). A CS associated with a sated US —that is, a US devalued by FSS—does not elevate systolic blood pressure. Lesions of the AMYG block conditioned systolic blood pressure responses to unsated, desirable foods regardless of whether the AMYG lesion is made before or after a CS has been trained (AX and preAX).

RESULTS

Figures 3, 4 and 5 demonstrated that model outputs replicate electrophysiological and behavioral results observed during unsignaled food reward presentation (US), Pavlovian conditioning (CS), and simultaneous visual discrimination (SVD). The simulations that are summarized in this section demonstrate how simulated lesions of the amygdala and orbitofrontal cortex impact reward devaluation on food consumption (Figure 7B), on the vigor of Pavlovian conditioned responding (Figure 7F), and choice behavior (Figure 8E).

Activations of model neurons replicate the electrophysiological profiles of neurons recorded from different brain regions during the performance of the US task (Figure 3). Food presentation is simulated by the activation of a gustatory input (Figure 3C). These gustatory inputs are passed to the lateral hypothalamus and rhinal cortex (Figure 1). In the lateral hypothalamus, taste-selective cells respond to gustatory inputs (Figures 5, 3D and 3F). The response of these LH cells is strongly modulated by the need for metabolites associated with each taste. As a consequence, LH cells in the model measure the drive to consume each taste (Figures 3E and 3G). Model US-selective drive-value category cells in the AMYG sum the taste-drive activity elicited from LH cells during US consumption and provide a measure of the drive to consume specific food rewards (Figure 3I).

Inputs from rhinal cells also modulate amygdala activity (Figure 5A). LH neurons generate systolic blood pressure responses related to US consumption and emotion (Figure 2, Smith et al., 1990; see also Figures 4D and 4H). ORB_m cells calculate the expected value of a food reward using drive value signals from the AMYG and reward identity information in the RHIN (Figures 3M and 3I). The activation of ORB_m cells determines consumption rate (Figure 2). The cortical masticatory areas (CMA) execute feeding behavior (Figure 2). Consumption rate in the model is altered by food-specific satiety (Figures 7B and 7D, 'CTL'). The value of new food rewards is learned in a dopamine-dependent fashion. Primary rewards are sensed in the LH, which sends signals via the PPTN (Figures 1, 3J and 3K) to elicit dopamine cell bursts in the VTA/SNc (Figures 3N and 3O).

In the CS task, visual stimuli learn to elicit conditioned Pavlovian approach and autonomic (systolic BP) responses (see Supplementary Notes 2). Figure 4B shows the model can learn to reliably generate a saccadic CR after multiple CS-US pairings (see Figure 4C for task and input timing). Learning the CS task depends on dopamine bursting responses produced in the SNc/VTA during US consumption (Figures 1 and 3O). These dopamine signals strengthen connections from the ORB_l and IT_a to the FEF. Inputs from ORB_l and IT_a cells to FEF cells drive saccadic responses (Figure 2). Figure 4B shows that neither lesions of the AMYG nor ORB_l disrupt the ability of the model to learn to generate a saccadic CR (Hatfield et al., 1996; Gallagher, et al. 1999). Inputs from the AMYG and ORB_l are needed to modulate the strength of conditioned responses (Figure 2; e.g., Figure 7F). Conditioned stimuli are presented as visual inputs and are recognized by visually-sensitive, stimulus-selective, IT_a cells (Figure 1). IT_a cells then relay these visual inputs to the ORB_l, AMYG, and FEF (Figure 2). The CS activates AMYG cells (Figure 4K) via a learned pathway from the IT_a (Figure 1). The US drive-value category cells in the AMYG that are activated by the CS interact with LH_out cells (Figure 5a) to calculate the expected value of a US given current needs (Figure 4I). LH_out cells also receive taste and drive inputs from LH_gus cells (Figure 5a) during US consumption (Figures 4G). Conditioned autonomic responses are also generated in response to CS-elicited activity in the LH (Smith et al., 1990; Figures 4D and 4E). ORB_l cells represent the expected value of a CS by combining stimulus identity information from the IT_a with US-related drive value information

from the AMYG (Figure 4M). ORB_l cells send inputs to the FEF that help determine the frequency and vigor of Pavlovian responses. As a consequence of these inputs from the ORB_l, saccadic CRs are modulated by changes in drive inputs (Figures 2 and 7F).

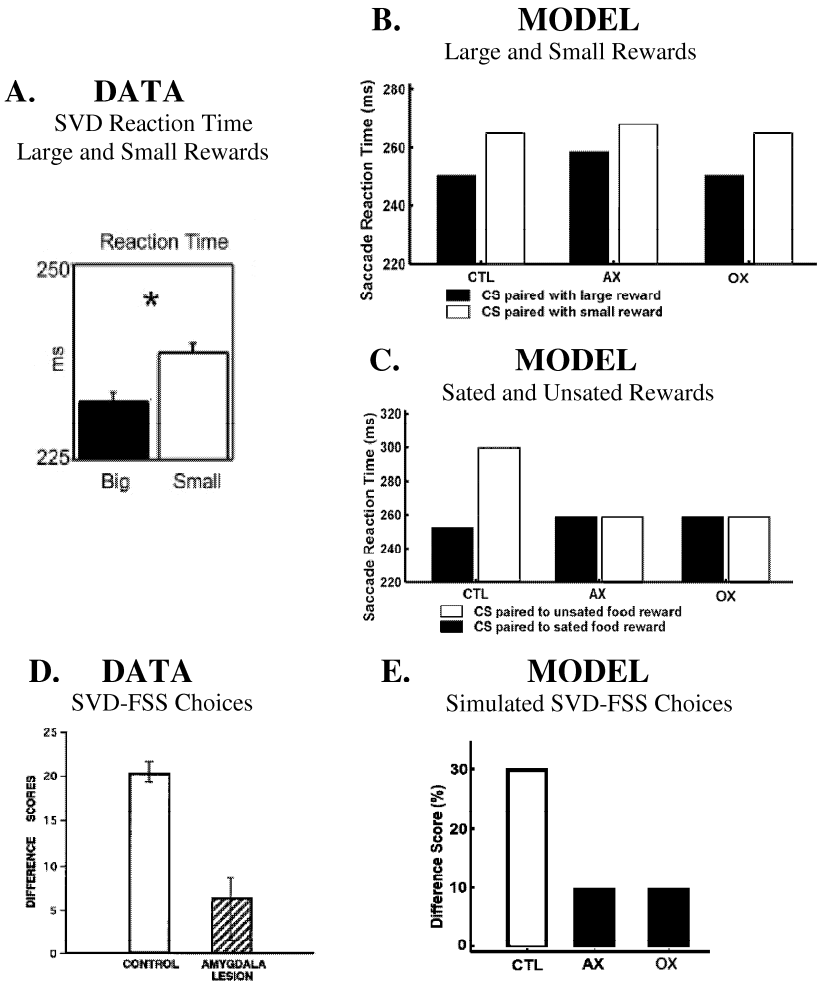

Figure 8: Reaction time, choice behavior, and reward value. (A) In the SVD task, saccadic reaction times are shorter on visual discrimination trials when the trial requires a monkey to discriminate between a CS predicting a big reward and a CS predicting no reward than when a monkey must discriminate between a CS predicting a small reward and a CS predicting no reward (reprinted with permission from Roesch and Olson, 2003). (B) Simulations of intact (CTL), AMYG lesioned (AX) and ORB_l lesioned (OX) models show shorter reaction times for saccades to visual cues associated with larger rewards than smaller rewards. Saccadic reaction time was determined when FEF cell activity exceeded a fixed threshold (see Methods for details). (C) Model predicts intact model (CTL) has a faster reaction time to a non-devalued than a devalued CS. Model predicts AMYG lesions (AX) and ORB_l lesions (OX) eliminate differences in reaction time to visual cues associated with sated and unsated rewards. (D) In the SVD-FSS task, an animal must choose between two conditioned stimuli associated with different food rewards. Choices made between the two CSs reflect preferences between the different food rewards. Devaluation of a US by food-specific satiety (FSS) shifts the choices of the animal away from cues associated with the devalued rewards (reprinted with permission from Malkova et al., 1997). Malkova et al. (1997) report the effects basolateral amygdala lesions using a difference score. The difference score is calculated by measuring the percent of the trials in which the to-be-devalued food is chosen over other foods, before and after FSS. The 'difference score' reflects the difference between these two percentages. (E) Using FEF activity to determine cue choice, the intact model (CTL) shows a similar shift in CS preference when the US associated with it is devalued by FSS. Food-specific satiety is implemented by lowering selected DRIVE inputs to the LH (see Figure 2). The automatic shifting of visual cue preference when an associated US is devalued by FSS is lost after AMYG lesions (AX) and ORB_l lesions (OX).

Figure 8B shows that the model is capable of learning the SVD task. The model learns to discriminate between the rewarded target and the unrewarded distractor within 10 trials (Figure 8B). The model learns to reverse such a learned contingency within a similar number of trials (Figure 8D). The SVD task poses the problem of how to assign value when there are competing visual stimuli. The model solves this problem by combining attentional feedback from the ORB_l to IT_a with competition between IT_a cells that recognize different visual stimuli (Figure 1; Grossberg, 1975; Grossberg and Levine, 1987). The attentional inputs from ORB_l enhance the salience of recipient stimulus representations in IT_a that are predictive of reward, while suppressing representations of irrelevant stimuli (Figure 8G). The degree of attentional enhancement reflects the value of associated rewards. The SVD task is strongly influenced by changes in the value of outcomes. When a reinforcer is devalued by food-specific satiety, the cues associated with that reinforcer will automatically devalue, resulting in a reliable, untrained, shift in stimulus preference. Figure 8E ('CTL') shows that when drive inputs are reduced to simulate reinforcer devaluation, cue preferences are noticeable different (where cue preference is measured by the percentage of different choices (Malkova, et al. 1997).

Amygdala and orbitofrontal lesions. Simulated lesions allow the model to address the question of whether conditioned stimuli rely on the amygdala or the orbitofrontal cortex to calculate the value of prospective rewards.

In Figure 7, bar graphs display the simulated and experimentally observed consequences of AMYG and ORB lesions for two measurable output variables: systolic BP responses and conditioned/unconditioned behavioral responses. Prior to any lesions, increasing the desirability or value of an expected reward increases the strength of conditioned and unconditioned systolic BP and behavioral responses. Following AMYG lesions, the capacity of autonomic and behavioral conditioned responses to revalue following a shift in reward value is lost. In contrast, following ORB lesions, only the capacity of conditioned behavioral responses to revalue following a shift in reward value is lost. The model proposes that these differential impairments occur because the AMYG and not the ORB plays the crucial role of calculating the value of prospective rewards. Hence AMYG lesions impair the adaptation of both conditioned autonomic and behavioral responses while ORB lesions only impair the ability of conditioned behavioral responses to adapt to changes in reward value (see Table 1).

In the US task, the data show that reward consumption elevates systolic BP responses in a manner sensitive to reward value (Figure 7C). The model also predicts that systolic BP responses are elevated when hunger is used to enhance the value of rewards (Figure 7D). In addition, the model replicates data showing AMYG and ORB lesions do not disrupt the sensitivity of systolic BP responses to the consumption of differently valued rewards (Figures 7C and 7D). The model predicts that these autonomic responses are spared because gustatory projections bypass the lesioned brain areas and directly activate the lateral hypothalamus to trigger a change in BP (Figures 2 and 5).

The value of a food reward also influences the amount of food consumed in the US task (Figure 7A). When a food reward is specifically devalued, data shows that consumption decreases in a food-specific manner, even after lesions of the AMYG or ORB_m (Figure 7A). The model replicates these observations (Figure 7B, 'AX', 'OX'). The model proposes the sensitivity of consumption responses to food specific satiety is intact because food-specific satiety has mechanisms that are independent of the amygdala and orbitofrontal cortex; namely, gustatory sensory habituation and post-ingestive changes in drive level (Figures 2 and 5).

In the CS task, the data shows visual cues associated with highly valued food rewards also generate increased blood pressure responses (Figure 7G). The model replicates these trends, predicts that systolic BP responses to visual cues are elevated when hunger is used to enhance the value of rewards or and associated cues (Figures 7D and 7H). Simulated lesions replicate and extend experimental observations. Simulated lesions replicate data showing that AMYG lesions (Figure 7H, 'AX') disrupt the revaluation of systolic BP responses to conditioned stimuli following the devaluation of rewards. In contrast, the model makes the novel prediction that ORB lesions do not impair this revaluation of systolic BP responses (Figure 7H, 'OX'). Lesions of the AMYG eliminate conditioned autonomic responses because the AMYG is a critical junction in the pathway linking visual stimuli with regions in the LH responsible for generating systolic BP responses (Figures 2 and 5). This pathway remains intact following ORB_l lesions (Figures 2 and 5). The inability of ORB lesions to disrupt differential autonomic responses to valued and devalued conditioned stimuli would provide evidence that reward value is calculated outside the orbitofrontal cortex.

In contrast to conditioned systolic BP responses, both model and data agree that lesions of the amygdala (Figures 7E and 7F, 'AX') and orbitofrontal cortex (Gallagher et al., 1999 ; Figure 7F, 'OX') disrupt the ability of Pavlovian approach responses to adapt to changes in the value of associated outcomes. ORB lesions disrupt the sensitivity of Pavlovian approach responses to the devaluation of rewards because these lesions prevent motor planning areas from accessing outcome-specific value information (Figures 2 and 5). AMYG lesions destroy the US-specific drive-value category cells in the AMYG, eliminating the inputs that provide ORB_l cells with an estimate of the current value of prospective outcomes (Figures 2 and 5). Without this AMYG input, the ORB_l cannot assign values to stimuli that reflect the current value of specific rewards. Hence, following AMYG lesions, motor planning areas such as the FEF (Figure 1) are also insensitive to outcome-specific changes in the value of conditioned stimuli.

The model clarifies how motor-planning regions, such as CMA and FEF, control learning and responding by combining reinforcement learning directed by dopaminergic signals calculated in the basal ganglia with outcome-specific information processed in the amygdala and orbitofrontal cortex (Figure 1). The model proposes that stimulus-response, or habit, learning relies on the strengthening of sensory-motor connections by dopamine signals. For example, in Figure 1, dopamine-gated learning strengthens stimulus-response associations between the IT_a and FEF, leading to the formation of response habits. In the habit learning system, reward value is calculated by the basal ganglia and broadcast by dopamine signals. These dopamine signals enforce the 'law of effect' and ensure reward value is encoded in stimulus-response associations (see Supplementary Equation Appendix).

In the outcome-specific learning system, reward-value can also be calculated online and attributed to stimuli by interactions between the ORB, AMYG and LH. Despite the fact that habit and outcome-specific learning systems are neurologically separable, model simulations show that reward-value information, whether encoded by habit or outcome-specific learning systems, exerts a similar effect on choice behavior and response latency. In the SVD task, reaction time gets shorter as reward magnitudes get larger (Figure 8A; Roesch and Olson, 2003). Using larger or smaller gustatory inputs to mimic reward size, the model replicates this trend (Figure 8B, 'CTL'). The model also replicates this trend when hunger and outcome-specific satiety are used to modulate reward value (Figure 8C, 'CTL'). Despite the similar consequences of these methods of modulating reward value, the model makes the prediction that amygdala and orbitofrontal lesions disrupt differences in response latency that result from outcome-specific

devaluation (Figure 8C, 'AX', 'OX'), but not those resulting from training the model with different reward magnitudes (Figure 8B, 'AX', 'OX'). In the model, different reward magnitudes alter reaction time by influencing the strength of connections between brain regions, whereas food-specific satiety alters reaction time by reducing the neural activation in brain regions associated with target selection. In the absence of the AMYG or ORB, repeated trials are needed for an animal to learn the new value of the stimulus and response, if reward value is altered (Corbit and Balleine, 2003). In the model, this type of habit or reinforcement learning is supported by dopaminergic signals that strengthen connections from the IT_a to the FEF (Figure 1).

Reinforcer devaluation. A second effect that differentiates habit learning and outcome-specific learning systems is the alteration of stimulus preference by reinforcer devaluation. Outcome-specific devaluation can yield reversals in stimulus preference without exposing a CS to the devalued US (Figure 8D; Malkova, et al. 1997). As with response latency, reversals in stimulus preference can also be encoded by the habit learning system (Figure 1), but such encoding requires repeated trials exposing stimuli and responses to new reward contingencies (Figure 4B). In the variant of the SVD task where stimulus preference is reversed by reinforcer devaluation, conditioned stimuli are associated with distinct food rewards and choices between conditioned stimuli reflect relative preferences for outcomes. When drive inputs (Figure 1) are decreased so as to devalue the preferred food reward, stimulus preferences will reverse (Figure 8E, 'CTL'). This occurs because drive inputs help determine the value of rewards (Figure 2). When the drive inputs associated with a given US decrease, the value of that US, as reported by US drive-value category cells in the AMYG, diminishes (Figure 2). In the SVD-FSS task, when the chosen reward is devalued, the US drive-value category cell representing a previously unchosen reward can become dominant and influence choice behavior. Signals sent along incentive motivational pathways allow the dominant US value category cells in the AMYG to boost the ORB_l incentive representation of the CS that is most strongly correlated with the preferred food reward. In turn, outputs from the ORB_l, to the FEF and IT_a bias the selection of targets for saccade.

Simulated lesions of the AMYG (Figure 8E, 'AX') or ORB_l (Figure 8E, 'OX') interrupt these pathways and render choice behavior insensitive to reinforcer devaluation. AMYG lesions destroy US-specific drive-value category cells, thereby disrupting choice behavior by blinding decision-making regions to the value of different prospective outcomes (Figure 2, 5). Orbitofrontal lesions prevent the animal from associating US value information with a particular CS, also disrupting choice behavior (Figure 2, 5).

Influence of lesions on second-order conditioning. The model addresses how simulated lesions of the amygdala and orbitofrontal cortex influence Pavlovian second-order conditioning. The ability of amygdala lesions to disrupt Pavlovian second-order conditioning depends on whether or not the conditioned reinforcer is trained before or after the amygdala lesion is performed (Figure 9A; Holland and Gallagher, 1999). The model replicates these observations. If the amygdala is lesioned before the conditioned reinforcer is trained, Pavlovian second-order conditioning fails (Figure 9A; Hatfield et al., 1996). If the amygdala is lesioned after the conditioned reinforcer is trained, Pavlovian second-order conditioning is unimpaired (Figure 9B; Setlow et al., 2002b).

The model predicts that AMYG lesions impair Pavlovian second-order conditioning by disrupting dopamine signaling (Figure 9E). Dopamine signals regulate learning in the model. Dopamine burst responses in the SNc/VTA enable IT_a representations of neutral visual stimuli to

associate with response and reinforcer representations in the FEF and AMYG (see Figures 1 and 5; Appendix Equation 7).

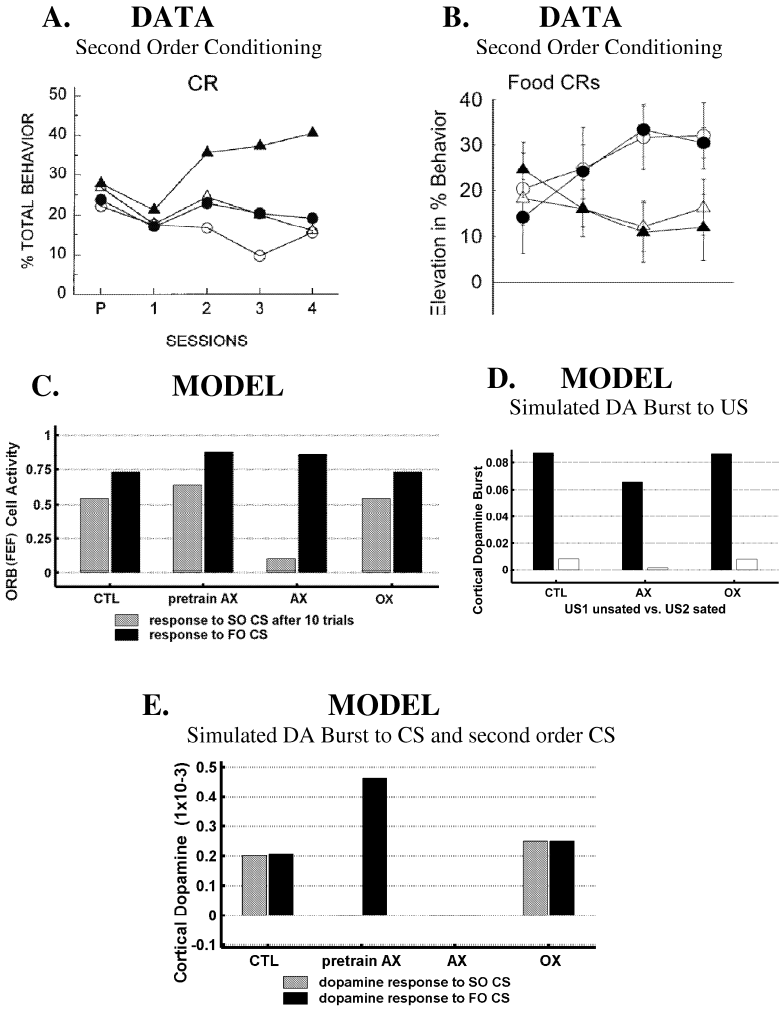

Figure 9: Second-order conditioning and conditioned dopamine responses. (A) The graph traces the increase in Pavlovian conditioned responses across four sessions of Pavlovian second-order conditioning (SOC). SOC is intact in control animals (closed triangles). However, second-order conditioning is impaired in animals with basolateral amygdala lesions, when the conditioned reinforcer is first trained after the amygdala lesions have been made (open triangles; reprinted with permission from Hatfield et al., 1996). Closed and open circles plot the frequency of CRs on trials where the second-order CS and conditioned reinforcer are unpaired. (B) Graph traces the increase in Pavlovian conditioned responses across four sessions of Pavlovian second-order conditioning (SOC). SOC is intact in control animals (open circles). Second-order conditioning is also intact in animals with basolateral amygdala lesions, as long as the conditioned reinforcer has been trained prior to making an amygdala lesion (closed circles; reprinted with permission from Setlow et al., 2002a). (C) Model Simulations reproduce these findings-- the SOC proceeds normally when the model is intact (CTL). SOC also proceeds normally after AMYG lesions as long as the CS was trained prior to making the AMYG lesion (pretrain AX). If the CS is not trained before the AMYG lesion is made (AX), SOC is impaired. (D) Simulations show that dopamine bursting responses to the consumption of food rewards is function in intact (CTL), AMYG-lesioned and ORB_l -lesioned variants of the model. In addition, lesions do not qualitatively effect the ability of satiety to modulate dopamine bursting responses. (E) Simulations show that the intact model (CTL) and the model with ORB_l lesions (OX) learn to produce dopamine bursting responses when first and second-order CSs are presented. AMYG lesioned models do not acquire dopamine responses to second-order conditioned stimuli (AX, pretrain AX), and only the pretrained AMYG lesion variant of the model has an intact dopamine response to a first-order CS.

The model predicts that first-order conditioning is not impaired by AMYG and ORB lesions (see Table 1, row 4) because US-related dopamine bursts are not impaired (Figure 9D). US-related dopamine bursting responses survive because gustatory inputs can drive these responses in the absence of the AMYG and ORB by activating the SNc/VTA via the LH and PPTN (Figures 2 and 5).

In order for second-order conditioning to occur, a CS must be an effective conditioned reinforcer. This means a CS must be able to elicit a conditioned dopamine burst response. This conditioned dopamine burst enables the second-order CS to learn to activate those AMYG, ORB_l and FEF cells activated when the conditioned reinforcer presentation. Using this principle, the model can explain the observation that AMYG lesions disrupt Pavlovian second-order conditioning when the conditioned reinforcer is trained after the lesion is made, but not when the CS is trained before the AMYG lesion is made (Figures 9A, 9B and 9C, 'AX' vs. 'pretrain AX').

When the AMYG is lesioned prior to training a CS, it blocks the ability of the CS to learn to elicit a conditioned dopamine burst (Figure 9E, 'AX'). CS-related dopamine bursting responses rely on excitatory signals being passed along a learned pathway linking the ORB_l to VS/VP and on to the PPTN and SNc/VTA (Figures 1 and 5). AMYG cells provide US value category inputs to the VS/VP that serve as teaching signals for CS-related signals from the ORB_l. As a consequence, if the AMYG is lesioned prior to training a CS, these teaching signals are removed and the CS cannot learn to elicit a conditioned dopamine burst. However, when the CS is trained prior to the AMYG lesion, the learned parallel pathway linking the ORB_l to the VS/VP is established (Figures 1 and 5) and the 'pretrained' CS can activate the SNc/VTA independently of the AMYG. Even after AMYG lesions, recovery-related changes ensure ORB_l cells remain sensitive to CS presentation in this parallel path (Schoenbaum, et al. 2003; see Equations 8, 9).

In contrast with AMYG lesions, simulations predict ORB_l lesions will not impair the learning of conditioned dopamine bursting responses by a first-order CS (Figure 9E, 'OX'). CS-related dopamine bursting responses are intact because, even after the ORB_l is eliminated, CS-related signals can continue to reach the SNc/VTA via the AMYG. With conditioned dopamine bursting responses intact, the model makes the novel prediction that Pavlovian second-order conditioning remains intact following ORB_l lesions (Figure 9C, 'OX').

DISCUSSION

The simulated lesion experiments reported in this study provide a behavioral fingerprint for the role that different model hypotheses play in reward evaluation, conditioning, and decision-making. Table 1 provides a summary of the behavioral impairments predicted by the model in comparison with those reported in the experimental literature. The remarkable agreement between these two sets of observations suggests that the model can be used to diagnose and understand the impairments in behavior and affect that result from lesions of the amygdala and orbitofrontal cortex. Table 2 summarizes the details of the experimental reports that are referenced in Table 1.

Several principles can be seen at work Table 1. First the experimental data show that the amygdala and orbitofrontal cortex are not needed for unconditioned stimuli to elicit basic autonomic and consumption responses. The model proposes this is the case because subcortical structures, especially the hypothalamus, regulate these responses and receive gustatory and drive signals directly, bypassing the amygdala and orbitofrontal cortex.

Task	Lesion Case							
	Intact	**AX**	**PreAX**	**OX**	**Model Intact**	**Model AX**	**Model PreAX**	**Model OX**
US Task								
US devalued by Food-specific satiety?	+(1)	+(1)	+(2)	+(3)	+	+	+	+
US consumption increases systolic blood pressure?	+(4)	+(4)	?	?	+	+	+	+
Consuming US causes dopamine burst?	+(5)	?	?	?	+	+	+	+
CS Task								
First order conditioning intact?	+(6)	+(6)	+(7)	+(3)	+	+	+	+
Presenting CS increases systolic blood pressure?	+(4)	-(4)	?	?	+	-	-	+
CS devalued when US devalued?	+(8)	-(8)	+(2)	-(3)	+	-	-	-
Presenting CS causes dopamine burst?	+(5)	?	?	?	+	-	+	+
Second order conditioning intact?	+(7)	-(7)	+(7)	?	+	-	+	+
Second order CS elicit dopamine burst?	+(9)	?	?	?	+	-	-	+
SVD Task								
Reward magnitude decreases reaction time?	+(10)	?	?	?	+	+	+	-
US devaluation increases reaction time?	?	?	?	?	+	-	-	-
CS preference altered by US devaluation?	+(11)	-(11)	?	-(12)	+	-	-	-

Table 1: Comparison of model lesions and experimental lesions. The table compares the results of simulated lesions of the amygdala and orbitofrontal cortex with experimental data. Results from experimental studies are shown with a white background. Results from model simulations are shown with a gray background. '+' is assigned to cells in the table where the expression of the property listed on the left hand side of the row is unimpaired. ' – ' is assigned to the cell if the listed property is impaired. '?' is assigned to those cells for which no experimental data are known. **Intact** indicates a control animal or simulation with no lesion. **AX** means the amygdala lesion was made before conditioning or other training commenced. **PreAX** indicates an amygdala lesion was made after the model or animal was trained on the particular problem. **OX** indicates the orbitofrontal cortex was lesioned before training. **1** (Corbit and Balleine, 2005); **2** (Pickens et al., 2003); **3** (Gallagher et al., 1999); **4** (Braesicke et al., 2005); **5** (Ljungberg et al., 1992); **6** (Holland and Gallagher, 1999); **7** (Setlow et al., 2002a); **8** (Hatfield et al., 1996); **9** (Waelti et al., 2001); **10** (Roesch and Olson, 2003); **11** (Malkova et al., 1997); **12** (Izquierdo et al., 2004).

Second, lesion experiments show the amygdala and orbitofrontal cortex do not play a large role in the acquisition and performance of approach CRs (Table 1, row 4). The persistence of autoshaping and other stimulus-response behaviors suggest habit learning involves brain structures that are relatively independent of the structures involved in emotional valuation systems, such as the ORB_l, ORB_m, AMYG, and LH (see Figures 1 and 2). These habit learning systems rely on the basal ganglia and dopamine signaling to reinforce associations between sensory regions such as IT_a or RHIN and motor regions such as the FEF or CMA (Figures 1 and 2). Previous models show in greater detail how dopaminergic and corticostriatal mechanisms accomplish this (Brown et al., 2004). In the current model, habit learning systems include FEF cells that control saccades via adaptively-weighted inputs from the IT_a and ORB_l. The adaptive weights on connections from the IT_a to the FEF and from the ORB_l to the FEF follow a dopamine-gated steepest descent learning law (see Equation 7). While dopamine reinforced associations between the IT_a and FEF are sufficient for generating behavioral CRs, they are not sufficient for explaining other aspects of CS processing. The ORB and AMYG are needed to explain conditioned systolic BP responses (Table 1, row 5), second-order Pavlovian CRs (Table 1, row 8), and how metabolic needs can selectively influence CS value (Table 1, rows 6 and 12).

In contrast to their limited role establishing approach CRs, the experimental data in Table 1 reveal that both the AMYG and ORB play an important role in tasks where conditioned Pavlovian and instrumental responses are modulated by the value of prospective rewards. In particular, the model proposes how the AMYG calculates the current value of expected rewards, and how the ORB_l assigns appropriate reward values to different stimuli.

In simulated Pavlovian tasks, the amygdala plays an important role in the learning of conditioned autonomic responses (see Table 1, row 5; Braesicke et al., 2005). This is an important result because the model makes the novel predictions that conditioned autonomic responses are graded by reward magnitude and unaffected by orbitofrontal lesions (Figures 7D and 7H; Table 1, row 5). This predicted dissociation provides a means to test the proposal that the amygdala and not the orbitofrontal cortex calculates current reward value.

Model simulations predict that both the brain regions underlying habit learning (e.g. IT_a and FEF) and affective learning (e.g. AMYG, LH, ORB_l) can influence saccadic reaction times in the SVD task. Dopamine signaling is sensitive to the magnitude of different rewards (Figure 9D; Fiorello, et al 2003) and reinforces stimulus-response activations that lead to reward. This ensures the adaptive weights on connections from the IT_a to the FEF reflect the relative magnitude of associated rewards and can influence saccadic reaction times in the SVD task. Because this memory is stored in the connections from the ITA to the FEF, lesions of the AMYG and ORB do not eliminate differences in saccadic reaction time (see Table 1, row 10). However, when reward value varies as a result of reinforcer devaluation, US-specific drive-value category cells in the amygdala, and their interactions with the lateral hypothalamus and orbitofrontal cortex, are needed to convey motivational information to response planning regions (Baxter et al., 2000; Izquierdo et al., 2004). As a consequence, model simulations make the novel prediction that AMYG and ORB lesions will eliminate differences in saccadic reaction time in the SVD task following changes in hunger or reinforcer devaluation.

Task	Independent Variable	Dependent Variable	Lesion Cases
US TASK			
(1) Corbit and Balleine, 2005	Food reward value: intact vs. devalued by FSS.	Number of food pellets consumed	CTL AX
(2) Pickens et al., 2003	Food reward value: intact vs. devalued by LiCl.	Number of food pellets consumed	Pre AX
(3) Gallagher et al., 1999	Food reward value: intact vs. devalued by LiCl.	Number of food pellets consumed	OX
(4) Braesicke et al., 2005	Presentation of preferred reward vs. nonpreferred reward.	Systolic BPR during US consumption	CTL AX
(5) Ljungberg et al., 1992	Presentation of juice reward.	SNc/VTA Dopamine cell activity	CTL
CS TASK			
(2) Pickens et al., 2003	Present CS paired with food reward vs. CS paired with food reward devalued by LiCl.	Frequency of approach CRs before and after	CTL Pre AX
(3) Gallagher et al., 1999	Present CS paired with food reward vs. CS paired with food reward devalued by LiCl.	Frequency of approach CRs before and after	OX
(8) Hatfield et al., 1996	Present CS paired with food reward vs. CS paired with food reward devalued by LiCl.	Frequency of approach CRs before and after	CTL AX
(4) Braesicke et al., 2005	Present CS paired with preferred reward vs. CS paired with nonpreferred reward.	Systolic BPR during CS presentation	CTL AX
(5) Ljungberg et al., 1992	Presentation of CS associated with juice reward US.	SNc/VTA Dopamine cell activity	CTL
SO-CS TASK			
(7) Setlow et al., 2002a	CS2-CS1 conditioning interleaved with CS1-US pairings.	Frequency of approach CRs during CS2	CTL AX Pre AX
(9) Waelti et al., 2001	Presentation of second order CS.	SNc/VTA Dopamine cell activity	CTL
SVD TASK			
(10) Roesch and Olson, 2003	Discriminate CS1 vs. CS0 and CS2 vs. CS0. Where CS0 is paired with no reward. CS1 with large reward, CS2 with small reward.	Latency for initiating a saccade to the rewarded CS	CTL
SVD-FSS TASK			
(11) Malkova et al., 1997	Forced choice between CS1 and CS2. Where CS1 and CS2 are paired with different foods. Compare choices before and after reinforcer paired with CS1 is devalued by satiety.	Frequency CS for reward 1 chosen over CS for reward 2	CTL AX
(12) Izquierdo et al., 2004	Forced choice between CS1 and CS2. Where CS1 and CS2 are paired with different foods. Compare choices before and after reinforcer paired with CS1 is devalued by satiety.	Frequency CS for reward 1 chosen over CS for reward 2	CTL OX

Table 2: Task references and description of experimental variables. The studies cited in Table 1 are grouped in the first column by experimental task. For each reference, the relevant experiment is summarized by describing the conditions that were manipulated by the experimenter (independent variable), the property that was observed during the experiment (dependent variable), and the lesion variants that were tested. Lesion abbreviations as in Table 1.

One experimental result from Table 1 is not reproduced by the model: When the amygdala is lesioned after a CS has already been conditioned, some preserved function is observed in the devaluation variant of the CS task. The data show that, if a CS is trained prior to lesioning the amygdala, the ability of conditioned responses to automatically adapt to devalued outcomes is spared (Pickens et al., 2003). The model, in contrast, predicts that the automatic devaluation of conditioned responses by food-specific satiety is lost following amygdala lesions, regardless of whether pretraining takes place (Table 1, row 6). One factor limiting the interpretation of this experiment for the model is that Pickens et al. (2003) relied on poisoning the food reward with lithium salts in order to devalue the food reward (Table 2), inducing a conditioned taste aversion (CTA). This form of devaluation relies on new learning that is known to be amygdala-independent and difficult to extinguish (Dunn and Everitt, 1988). In contrast, devaluing a US by satiety is reversible, involving a motivational shift rather than new learning (Corbit and Balleine, 2003). We suggest that the recovery of function observed by Pickens et al. (2003) is peculiar to cases where CTA has been used to devalue the US and may involve a similar recovery process as that by which the model predicts preservation of second-order conditioning following amygdala lesions. Repeating these experiments using food-specific satiety to devalue rewards is probably the most direct way to test whether the devaluation of food rewards by lithium poisoning and satiety rely on the same or different neural circuits.

Experimental data show that the ability of a conditioned stimulus to act as a conditioned reinforcer is impaired following amygdala lesions (Table 1, row 8; Hatfield et al., 1996; Setlow et al., 2002a). Experiments also reveal that, if the CS is trained prior to the amygdala lesion being made, the ability of the CS to function as a conditioned reinforcer and to induce secondary conditioning is intact (Table 1, row8). This preserved function relies on pathways through the ventral striatum (Setlow et al., 2002b). In the model, US-specific drive-value category cells in the amygdala project to the ventral striatum, providing teaching signals for inputs from the ORB_l (Figure 1). When the model is trained prior to amygdala lesions, connections between the orbitofrontal cortex and US-specific ventral striatal cells learn to reflect US value and compensate for the loss of the amygdala. Recovery of second-order conditioning occurs because this 'pretraining' establishes a learned pathway from the ORB_l to the ventral striatum that enables the CS to trigger a dopamine burst.

If, following conditioned taste aversion, the preservation of CS sensitivity to US devaluation relies on a similar pathway from the ORB_l to US-specific representations in the ventral striatum, combined lesions of the amygdala and ventral striatum could be used to test this. This lesion scenario would be diagnostic because, after pretraining, neither lesions of the ventral striatum alone nor amygdala alone should disrupt performance in the reward devaluation task.

The predictions of the model match well with the clinical observations of Bechara et al. (1999). However, some discrepancies exist. As expected from the model, Bechara and colleagues (1999) found that patients with amygdala lesions lacked autonomic (SCR, skin conductance response) responses to conditioned reinforcers (money credits on a computer screen) and other conditioned stimuli presented during a gambling task. However, patients with orbitofrontal lesions were observed to have some impairments in the ability to generate autonomic (SCR) responses. In agreement with the model, orbitofrontal patients had an intact autonomic response during the presentation of conditioned reinforcers. However, orbitofrontal patients also lacked the anticipatory autonomic (SCR) responses observed in control subjects when they were choosing between two risky decks of cards These observations suggest that the orbitofrontal

cortex may play a more significant role influencing emotion and autonomic state in gambling tasks than is so-far captured by the model. In particular, when patients gamble, they may rely on working memory to generate hypotheses about the consequences of different choices (Bunge, et al. 2005; Grossberg and Pearson, 2007). It seems likely that the orbitofrontal cortex is needed for items being processed in working memory to acquire emotional relevance.

Some results from the MOTIVATOR model contrast with competing theories of these brain regions in these and related tasks. Frank and Claus (2006) looked at decision-making in similar tasks, but with a model designed to explain the interaction of orbitofrontal cortex and the basal ganglia in the context of instrumental learning and gambling tasks. Although they also asserted that their model is capable of explaining outcome-specific learning, their analysis of outcome-specific learning was critically flawed. They did not correctly represent or treat the structure and purpose of reward devaluation tasks. In the reward devaluation variants of the SVD and CS tasks, reward devaluation takes place outside of the task, away from any of the conditioned stimuli presented during the task (Malkova et al., 1997; Hatfield et al., 1996), whereas Frank and Claus (2006) assumed that the CS must be paired with the US in its newly devalued state before any transfer of devaluation to the CS would occur. However, the whole point of the devaluation task is that additional CS-US pairing is not needed: The reward is devalued and then responses to the CS revalue automatically, even when measured in extinction, so that there never is the opportunity for the CS to learn the new value of the US (Malkova et al., 1997; Balleine and Killcross, 1994). The MOTIVATOR model is consistent with these data because it simulates the SVD task with devaluation as a consequence of automatic revaluation that relies on stimulus-outcome associations involving the ORB_l and drive-value category cells in the AMYG and not simple stimulus-response associations learned by habit between the IT_a and FEF using dopamine bursts as reinforcement signals.

In summary, the MOTIVATOR model proposes how parallel dopaminergic and affective value systems interact to modulate behavior and attention during learning, extinction, and reversal. Simulated lesion studies illustrate how these claims might be verified. The model predicts that impairments in the ability of conditioned stimuli to evoke dopamine burst responses underlie the impairments in Pavlovian second-order conditioning observed after amygdala lesions. The model also demonstrates that amygdala lesions disrupt conditioned affect while orbitofrontal lesions disconnect affect from stimuli and behavior, leaving dopaminergic habit and emotional learning systems intact but unable to interact.

SUPPLEMENTARY MATERIAL

Supplementary Notes 1

When a food is presented, the appropriate pattern of GUS inputs is activated and this pattern is recognized by food category cells in the rhinal cortex (RHIN). GUS inputs also directly activate taste-drive cells in the lateral hypothalamus (LH_gus cell; Figures 3E and 5) that sense the levels of metabolites that correspond to each GUS taste. The food category RHIN cells then prime US drive-value category cells in the amygdala (AMYG) and US-selective ORB_m cells. Interactions between the AMYG and LH cells calculate the value of a specific food reward relative to the current needs of the animal. ORB_m cells use the food value information calculated in the AMYG, and the food identity information represented in the RHIN, and drive food-specific consumption in proportion to expected value. A blood pressure (BP) signal is activated by lateral hypothalamic output cells (LH_out); see Figure 5. Dopamine bursting responses are generated directly by LH_gus cells and indirectly by AMYG cells.

Supplementary Notes 2

When a CS is presented, it activates a visual input pattern that is recognized by object category cells in the anterior inferotemporal cortex (IT_a). These IT_a cells activate correlated US-selective AMYG cells and associated CS-selective ORB_l cells (Figure 4M) When an AMYG cell is activated by a CS, it interacts with LH cells to calculate the expected value of the associated US. In particular, top-down inputs from the AMYG substitute for GUS inputs and activate those LH cells normally activated during US consumption (Figure 4I). The magnitude of the response of LH_gus cells to these top-down inputs is modulated by bottom-up drive input signals (Figure 4G). Return projections allow AMYG cells to sum LH cell activity and estimate the current value of the expected food reward. These top-down projections from the AMYG to the LH also drive emotional responses to conditioned stimuli such as blood pressure (BP). ORB_l cells use the US value information calculated in the AMYG and the CS identity information represented in the IT_a to trigger conditioned responses. CS-related dopamine bursting responses are elicited by projections from the AMYG to the LH and ventral striatum (VS). In the CS task, US-related dopamine signals come under the control of the basal ganglia reward expectation filter (Figure 1). The basal ganglia learn to predict the timing of reward presentation relative to CS-related signals represented in the ORB_l. Once trained, the basal ganglia are capable of generating an adaptively timed inhibitory signal that attenuates US-related dopamine burst responses or signals US omission with a dip in dopamine response levels. The basal ganglia can learn to generate such a response within twenty CS-US pairings (Hollerman and Schultz, 1998).

Supplementary Notes 3

In the simplest case of the SVD task, two visual inputs are presented. Different stimulus-selective IT_a cells recognize and respond to each visual input (Figure 5F). The IT_a cell that selectively recognizes the CS activates the AMYG cell corresponding to the US with which the CS has been associated. The US-specific AMYG cell calculates the value of the expected food reward. Stimulus-selective ORB_l cells then use US value information calculated in the AMYG and the CS identity information represented in the IT_a to calculate to expected value associated with each visual stimulus. The CS-selective ORB_l cell is most strongly activated by inputs from the IT_a and AMYG. The activated ORB_l cell enhances the sensory representation of the CS in IT_a via a positive feedback loop, suppressing the sensory representation of the distracting visual stimulus. In addition, the ORB_l cell sends feedforward projections to the FEF, which speed

saccade planning and reaction time. In addition to incentive activations in the ORB_l, dopamine bursting responses are elicited by CS presentation.

In the variant of the SVD task where a decision is made between two stimuli associated with different rewards, the dynamics are similar. When the visual stimuli are presented, each CS is recognized by a different IT_a cell. The IT_a cells then project to different US value category cells in the AMYG that code for the food rewards with which each CS has been trained. The AMYG cells calculate the expected value of each food reward via its interactions with the LH. The AMYG cell with the greatest activation significantly, though not completely, suppresses the activation of the competing AMYG cell. CS-selective ORB_l cells receive this US value information from the AMYG and link it to CS-identity information from the IT_a. Using mechanisms discussed above, the ORB_l cell with the greatest activity enhances the IT_a representation of its favored CS, suppresses the competing CS, and helps generate a saccade to its favored CS. Dopaminergic bursting responses and emotional signals (blood pressure) are also generated via the subcortical routes discussed previously.

Supplementary Notes 4

The CogEM model describes the minimal anatomy capable of motivated learning. The model has clarified many data about conditioning, notably the relations of sensory cortex, amygdala, and prefrontal cortex (Grossberg, 2000). In CogEM, the unit of long-term memory (LTM) is a spatial pattern of adaptive weights that is distributed across multiple synaptic connections. A stimulus-sampling operation alters LTM via learning rules that describe how connections between neurons change to encode stimulus-related activity (see Equations 6,7 and 36-44 in the Supplementary Equation Appendix). CogEM is designed to cope with the basic fact that learning can occur even if the time intervals between CS and US presentation on successive learning trials can differ. One contributing factor is that the model's short term memory (STM) equations describe activities that decay slowly (see Equations 1-4), ensuring a trace of CS- or US-related activity can overlap even when the bottom-up CS and US inputs themselves do not. CogEM shows how variable CS-US intervals combined with the obvious fact that, after learning, the CS alone can elicit a CR on performance trials can greatly constrain the learning circuit (Grossberg, 1971). In the model, this postulate is met by ensuring that connections from the IT_a and AMYG can activate the ORB_l, which in turn can activate the FEF (Equations 10-12, 48). CogEM also models how a given cue can be associated with any of several drive states. The model realizes this postulate by incorporating connections that link the IT_a with the AMYG, which controls motivational and autonomic arousal (Equation 12). CogEM models how behavior is influenced by an organisms drives by connecting drive areas such as the AMYG to the ORB_l and ORB_m, which influence the vigor of motor responses in the FEF (Equations 11,48). A given incentive can be associated with any of several external cue representations. The model realizes this postulate by the learning of subliminal motivational sets: AMYG cells associate with ORB_l and ORB_m cells via incentive motivational learning (Equations 36 and 41). A discriminative cue can elicit distinct responses in different motivational contexts. In CogEM, drive inputs represent different specific hungers that can enhance the value of different food rewards. In the SVD task, these different drive inputs alter choice behavior. To explain how motivationally incompatible behaviors compete, cues associated with different drives compete in the AMYG and LH. Owing to feedback within the drive representations, this competition takes into account both sensory and drive strength to make a motivational decision and thereby represents a motivational heterarchy (Equations 12, 15-17). The onset of an aversive event can suppress new reinforced learning, whereas the offset

of an aversive event can trigger new reinforced learning. In the model, an aversive input can suppress new learning of appetitive cues by competition in incentive and drive representations. A gated dipole in the drive representation enables the offset of an aversive event leads to a motivational rebound that can trigger new appetitive reinforcement learning by eliciting a dopamine spike. Due to this motivational rebound, offset of a conditioned reinforcer can trigger reinforcer properties of the opposite sign. Owing to parameters and inputs, this occurs more easily for aversive than appetitive stimuli. Effective regulation of motivated attention and decision-making is facilitated by the property that total activity across the internal representations of sensory cues tends to be conserved, or normalized. In the model this is implemented by contrast normalization of IT_a and RHIN activities using a feedforward shunting on-center off-surround network of interactions across visual or gustatory sensory representations (Equations 4, 10, and 18). CogEM also ensures that the persistence of learned meanings during parallel processing of motivationally incompatible cues is possible. In other words, environments which include motivational incompatible cues, such as cues for food and sex, do not lead to rapid cross-conditioning of cue-drive associations. This could easily occur in any purely feedforward conditioning model. In CogEM, this problem is ocvercome by protecting conditioned reinforcer learning from the IT_a and RHIN to the AMYG (Equations 38 and 39) by attentional mechanisms linking the ORB_l to IT_a and ORB_m to RHIN (Equations 10 and 11), thereby focusing selective attention upon one motivational alternative at a time, and by gating learning to times when the corresponding drive representation is active by using dopaminergic signals (Equations 32,33).

Supplementary Notes 5

Behavioral studies show when multiple appetitive stimuli are presented, they interact in an additive fashion, enhancing approach responses. The same is true for avoidance behavior when multiple aversive stimuli are presented. In contrast, interactions between appetitive and aversive stimuli are suppressive, reducing response levels (Weiss et al., 1996; Dickinson and Balleine, 2001). The gated dipole captures these phenomena by segregating appetitive and aversive signals into specialized ON and OFF channels that process signals of the opposite affective valence. Feedforward inhibition between these ON and OFF channels results in competitive interactions that suppress opponent affective activations. In addition to opponent interactions, behavioral studies reveal that animals can habituate to chronic affective signals and experience rebound phenomena such as the relief that accompanies the offset of pain or fear (Grossberg, 1972, 1975; Dickinson and Dearing, 1979). The model captures these phenomena by gating signals in each of the opponent channels with an activity-dependent habituating transmitter gate. These habituating transmitter gates adapt to the sum of tonic and phasic appetitive or aversive inputs. The model can produce rebound phenomena by incorporating a nonspecific arousal signal that arouses both ON and OFF channels. When a phasic signal is presented, it habituates the corresponding transmitter gate more than the transmitter in the opponent channel. When the phasic signal shuts off, the opponent channel has a momentary competitive advantage during the time interval when the more habituated transmitter gate recovers. During this time, the tonic nonspecific input to opponent channels can generate a phasic rebound signal. Sudden novelty-sensitive increases or bursts in arousal can also generate rebound signals in opponent channels (Grossberg, 1972, 1984).

Supplementary Equation Appendix

A.1 Short Term Memory Equations.

A.1.1 IT_a STM Equations. IT_a cell activities, I_j, model visually-sensitive, cue-selective cells in the anterior inferotemporal cortex. The subscript *j* indexes the different visual object categories coded by cells in IT_a. IT_a cells are modeled by an attentive shunting network (3) that receives bottom-up driving VIS inputs C_j and top-down attentive ORB_l inputs, O_{ji}^L:

$$\tfrac{1}{10}\dot{I}_j = -I_j + (1-I_j)\left(6C_j\left(1+2\sum_i O_{ji}^L\right)\right) - (0.2+I_j)\left(9\sum_{k\neq j} C_k + 17\sum_{k\neq j,i} O_{ki}^L\right). \tag{10}$$

By (10), I_j passively decays at rate 1 via term $-I_j$. The excitatory and inhibitory shunting terms $(1-I_j)$ and $-(0.2+I_j)$, respectively, bound cell activity within the interval [-0.2, 1]. The driving excitatory input is $6C_j$. The top-down modulatory excitatory ORB_l inputs are $2\sum_i O_{ji}^L$. The summation over index ***i*** enables appetitive and aversive ORB_l inputs to enhance salience equally. The inhibitory driving off-surround terms are $9\sum_{k\neq j} C_k$ and $17\sum_{k\neq j}\sum_i O_{ki}^L$.

A.1.2 ORB_l *STM Equations.* ORB_l cell activities, O_{ji}^L, model object-value orbitofrontal cells that respond selectively to motivationally supported visuosensory cells (Hosokawa et al., 2004). Subscript *i* indicates whether the cell is appetitive or aversive and subscript *j* indicates the IT_a visual category that the ORB_l cell prefers. ORB_l cells are modeled by an attentive shunting network that receives bottom-up driving IT_a inputs, I_j, and top-down attentive modulatory AMYG inputs, A_{ri} (Amaral and Price, 1984):

$$\begin{aligned}\tfrac{1}{50}\dot{O}_{ji}^L = \; & -O_{ji}^L + (1-O_{ji}^L)\left(0.1\left[I_j\right]^+\left(1+160\sum_r W_{jri}^{AO}\left[A_{ri}\right]^+\right)\right) \\ & -(O_{ji}^L)\left(2\sum_{k\neq j}\sum_r W_{kri}^{AO}\left[A_{ri}\right]^+ + 0.2\sum_{k\neq j}\left[I_k\right]^+ + 50\sum_{l\neq i}\left[O_{jl}^L\right]^+\right).\end{aligned} \tag{11}$$

By (11), O_{ji}^L passively decays at rate 1 via term $-O_{ji}^L$. The excitatory and inhibitory shunting terms $(1-O_{ji}^L)$ and $-(O_{ji}^L)$, respectively, bound cell activity within the interval [0, 1]. The bottom-up excitatory driving IT_a input is $0.1\left[I_j\right]^+$. The output signal function $\left[I_j\right]^+$ rectifies I_j at a zero threshold, passing only non-negative values of I_j. The top-down modulatory excitatory attentive input is $160\sum_r W_{jri}^{AO}\left[A_{ri}\right]^+$, where the W_{jri}^{AO} are LTM weights that learn to map US-specific AMYG cells, (*r, i*), to CS-specific ORB_l cells, *j*, where *r* denotes the *r*-th AMYG category and *i* whether it is appetitive (*i* = 1) or aversive (*i* = 2). The driving inhibitory off-surround inputs from IT_a and AMYG are $0.2\sum_{k\neq j}\left[I_k\right]^+$ and $\sum_{k\neq j}\sum_r W_{kri}^{AO}\left[A_{ri}\right]^+$, respectively. In addition, there is opponent inhibition between appetitive and aversive ORB_l cells, $50\sum_{l\neq i}\left[O_{jl}^L\right]^+$.

A.1.3 AMYG STM Equations. AMYG cell activities, A_{ri}, model multimodal, US-selective cells found in the basolateral amygdala (Nishijo et al., 1988a, 1988b). The subscript *r* identifies the *r*-th US-specific affective category and the subscript *i* indicates whether the cell is appetitive or aversive. AMYG cells are modeled by attentive shunting networks that receive bottom-up excitatory driving LH_out cell inputs, H_{si}^{O}, and top-down attentive modulatory excitatory inputs from IT_a cells, I_j, and RHIN cells, R_t:

$$\begin{aligned}\tfrac{1}{50}\dot{A}_{ri} = \; & -A_{ri} + \left(1 - A_{ri}\right)\left(\sum_s W_{sri}^{HA}\left[H_{si}^{O}\right]^+\left(0.3 + 13\sum_j W_{jri}^{IA}\left[I_j\right]^+ + 13\sum_t W_{tri}^{RA}\left[R_t\right]^+\right) + 150 f\left(A_{ri}\right)\right) \\ & -\left(0.2 + A_{ri}\right)\left(0.25\sum_{u\neq r}\sum_s W_{usi}^{HA}\left[H_{si}^{O}\right]^+ + 250\sum_{u\neq r} g\left(A_{ui}\right)\right).\end{aligned} \tag{12}$$

By (12), A_{ri} passively decays at rate 1 via term $-A_{ri}$. The excitatory and inhibitory shunting terms $\left(1 - A_{ri}\right)$and $-\left(0.2 + A_{ri}\right)$, respectively, bound cell activity within the interval [-0.2, 1]. The driving excitatory LH_out input is $\sum_s W_{sri}^{HA}\left[H_{si}^{O}\right]^+$. The excitatory modulatory inputs are from the IT_a, $13\sum_j W_{jri}^{IA}\left[I_j\right]^+$, and the RHIN, $13\sum_t W_{tri}^{RA}\left[R_t\right]^+$. The W_{rsi}^{HA} are LTM weights that associate LH drive features with US-specific AMYG categories. Weights W_{jri}^{IA} and W_{tri}^{RA} are LTM weights that map CS-specific IT_a cells and US-specific RHIN cells to US-specific AMYG cells, respectively. The driving inhibitory off-surround LH_out input is $0.25\sum_{u\neq r}\sum_s W_{usi}^{HA}\left[H_{si}^{O}\right]^+$. Equation (12) also includes recurrent excitation $150 f\left(\left[A_{ri}\right]^+\right)$ and inhibition $250\sum_{u\neq r} g\left(\left[A_{ui}\right]^+\right)$. The recurrent excitatory signal function, *f*, ensures strong feedback amplification for small values of A_{ri} between [0, 0.025], but progressively less amplification above 0.025:

$$f(A_{ri}) = \begin{cases} 0 & \text{if} \quad A_{ri} \le 0 \\ \left(A_{ri}\right)^2 & \text{if} \quad 0 < A_{ri} \le 0.025 \\ \left(A_{ri}\right)^2 e^{-1000\left(A_{ri} - 0.025\right)} & \text{if} \quad A_{ri} > 0.025. \end{cases} \tag{13}$$

The recurrent inhibitory signal function, *g*, is:

$$g\left(A_{ui}\right) = \begin{cases} 0 & \text{if} \quad A_{ui} \le 0 \\ \left(A_{ui}\right)^2 & \text{if} \quad A_{ui} > 0. \end{cases} \tag{14}$$

For values of A_{ri} in the interval [0, 0.025], the recurrent signal functions (13) and (14) support fast contrast enhancement among competing AMYG cells. As a result, a single winner is chosen. Outside this interval, recurrent inhibition $g\left(\left[A_{ui}\right]^+\right)$ continues to grow quadratically to maintain suppression of the losers, whereas recurrent excitation is negligible. This allows choice without a loss of analog sensitivity so that the activity level of the AMYG winner closely tracks the amplitude of its non-recurrent inputs.

A.1.4 LH_in STM Equations. LH cells, taken together, form an array of recurrent gated dipole opponent processing circuits wherein metabolic, sensory reinforcer, and amygdala

category signals converge. LH input cell activities, H_{si}^{I}, model LH cells that reflect the identity and concentrations of specific nutrients (Karadi et al., 1992); see Figure 5a. The subscript *s* indexes the metabolic features processed by the LH_in cell. The subscript *i* = 1, 2 indicates whether the cell is appetitive or aversive. LH_in cells receive metabolic inputs M_{si}, arousal inputs α_1, and LH_out cell feedback signals, H_{si}^{O} (see Equation 17):

$$\tfrac{1}{50}\dot{H}_{si}^{I} = -H_{si}^{I} + 0.05M_{si} + 0.25\alpha_1 + 0.35\left[H_{si}^{O}\right]^{+}. \tag{15}$$

Activity H_{si}^{I} passively decays at rate 1 via term $-H_{si}^{I}$. Additive equations are used and remain bounded because the inputs are bounded.

A.1.5 LH_gus STM Equations. LH_gus cell activities, H_{si}^{G}, model taste-responsive LH drive-specific cells (Karadi et al., 1992). Each cell is indexed by homeostatic features, *s*, and affective valence, ***i*.** LH_gus cells receive driving inputs from LH_in cells, H_{si}^{I}, and modulatory GUS inputs, G_m:

$$\tfrac{1}{50}\dot{H}_{si}^{G} = -H_{si}^{G} + 5Y_{si}\left(\left[H_{si}^{I}\right]^{+}\right)\left(1 + 0.6W_{msi}^{GH}X_m G_m\right). \tag{16}$$

Activity H_{si}^{G} decays at rate 1 via term $-H_{si}^{C}$. The excitatory driving inputs are $4Y_{si}\left[H_{si}^{I}\right]^{+}$. Y_{si} is a habituative transmitter that gates H_{si}^{I} input signals; see Equation (34). In the excitatory modulatory gustatory inputs $0.6W_{msi}^{GH}X_m G_m$, the taste-specific habituative term X_m gates gustatory inputs, G_m (see Equation 35). W_{msi}^{GH} are fixed weights that map tastes to drive features in a one-to-one fashion.

A.1.6 LH_out STM Equations. LH output cell activities, H_{si}^{O}, model LH cells that generate opponent responses to appetitive and aversive cues and rewards (Ono et al., 1986). Each cell activity is indexed by homeostatic features, *s* and affective valence, *i*:

$$\begin{aligned}\tfrac{1}{50}\dot{H}_{si}^{O} = \; & -H_{si}^{O} + \left(1 - H_{si}^{O}\right)\left(1.75\left[H_{si}^{G}\right]^{+}\left(1 + 1.75\sum_{r} W_{sri}^{AH}\left[A_{ri}\right]^{+}\right)\right) \\ & -\left(1 + H_{si}^{O}\right)\left(\left[H_{S}^{G}\right]^{+} + 0.25\sum_{u\neq s}\left[H_{ui}^{G}\right]^{+} + 0.5\sum_{u\neq s}\sum_{r} W_{rui}^{AH}\left[A_{ri}\right]^{+}\right).\end{aligned} \tag{17}$$

The excitatory and inhibitory shunting terms $\left(1 - H_{si}^{O}\right)$ and $-\left(1 + H_{si}^{O}\right)$ in (17) bound cell activity within the interval [-1, 1]. LH_gus cells provide bottom-up excitatory driving inputs $1.75\left[H_{si}^{G}\right]^{+}$. The top-down attentive excitatory modulatory input from AMYG categories is $1.75\sum_{r} W_{sri}^{AH}\left[A_{ri}\right]^{+}$. The W_{sri}^{AH} are LTM weights that map US-specific AMYG category cell outputs to US-related metabolic features in LH_out cells. Summation over *r* occurs across US-specific AMYG category cells. Inhibitory driving off-surround terms are from AMYG categories $0.5\sum_{u\neq s}\sum_{r} W_{rui}^{AH}\left[A_{ri}\right]^{+}$ and from LH_gus cells $0.25\sum_{u\neq s}\left[H_{ui}^{G}\right]^{+}$**.** These inhibitory inputs suppress LH_out cells at which there is a poor match between top-down attentive signals from AMYG and bottom-up driving input signals from LH_gus cells. LH_gus cells provide an

additional driving inhibitory input H_S^G that introduces opponent inhibition between an opponent pair, H_{si}^O and H_S^O, of drive channels. In all, the two types of inhibition link the various LH opponent circuits into a gated dipole field (Grossberg 1972b, 1984; Olson and Grossberg, 1994).

A.1.7 RHIN STM Equations. RHIN cells activities, R_t, model reward-selective, multimodal neurons that are proposed to exist in the rhinal cortex (Parker and Gaffan, 1998). Subscript *t* indexes the multimodal US category favored by the *t*-th RHIN cell. RHIN cells are modeled using attentive shunting networks and receive bottom-up excitatory driving inputs from IT_a cell activities, I_j and GUS cell activities, G_m. Top-down modulatory excitatory inputs arise from ORB_m inputs, O_{ti}^M:

$$\begin{aligned} \tfrac{1}{10}\dot{R}_t = \; & -R_t + (1-R_t)\left(\left(0.4\sum_j W_{jt}^{IR}\left[I_j\right]^+ + 5\sum_k W_{mt}^{GR}G_m\right)\left(1+2\sum_i\left[O_{ti}^M\right]^+\right)\right) \\ & -(0.2+R_t)\left(3\sum_{u\neq t}\sum_j W_{ju}^{IR}\left[I_j\right]^+ + 5\sum_{u\neq t}\sum_m W_{mu}^{GR}X_mG_m + 6\sum_{u\neq t}\sum_i\left[O_{ui}^M\right]^+\right). \end{aligned} \tag{18}$$

The excitatory and inhibitory shunting terms $(1-R_t)$ and $-(0.2+R_t)$, respectively, bound cell activity within the interval [-0.2, 1]. The driving excitatory inputs are $0.5\sum_j W_{jt}^{IR}\left[I_j\right]^+$ and $5\sum_{u\neq t}\sum_m W_{mu}^{GR}X_mG_m$. The terms W_{jt}^{IR} and W_{mt}^{GR} are weights that allow RHIN cells to respond selectively to gustatory and visual features of particular unconditioned stimuli. Learning of the W_{jt}^{IR} and W_{mt}^{GR} LTM weights is not treated in this paper, but could be done, for example, using mechanisms in Carpenter and Grossberg (1991). The modulatory ORB_m excitatory input is $2\sum_i\left[O_{ti}^M\right]^+$. Summation over the subscript, *i*, indicates that both appetitive and aversive inputs from the ORB_m enhance salience. The driving inhibitory GUS, IT_a, and ORB_m off-surround inputs are $5\sum_{u\neq t}\sum_m W_{mu}^{GR}X_mG_m$, $3\sum_{u\neq t}\sum_j W_{ju}^{IR}\left[I_j\right]^+$, and $6\sum_{u\neq t}\sum_i\left[O_{ui}^M\right]^+$, respectively.

A.1.8 ORB_m *STM Equations.* ORB_m cell activities, O_{ti}^M, model reward-selective, motivationally-sensitive neurons in the orbitofrontal cortex (Tremblay and Schultz, 2000a, 2000b). As a consequence of their anatomical connections, ORB_l cells represent the approach or avoidance value of visual stimuli while ORB_m cells represent the consumption value of rewards (Small et al., 2007); see Fig. 1. Subscript *t* labels the US category in the RHIN to which the ORB_m cell responds and the subscript *i* labels whether the cell is appetitive or aversive. ORB_m cells are modeled using attentive shunting networks that receive bottom-up driving excitatory RHIN signals, R_t and attentive top-down modulatory excitatory AMYG inputs, A_{ri} (Amaral and Price, 1984):

$$\begin{aligned}\tfrac{1}{50}\dot{O}_{ti}^{M} = \; & -O_{ti}^{M} + (1-O_{ti}^{M})\left(0.02\left[R_t\right]^{+}\left(1+200\sum_{r} W_{tri}^{AM}\left[A_{ri}\right]^{+}\right)\right) \\ & -\left(O_{ti}^{M}\right)\left(6\sum_{u\neq t}\sum_{r} W_{rui}^{AM}\left[A_{ri}\right]^{+} + 0.2\sum_{u\neq t}\left[R_u\right]^{+} + 15\sum_{j\neq i} O_{tj}^{M}\right).\end{aligned} \tag{19}$$

The excitatory and inhibitory shunting terms $(1-O_{ti}^{M})$ and $-(O_{ti}^{M})$, respectively, bound cell activity within the interval [0, 1]. The bottom-up excitatory driving RHIN input is $0.02\left[R_t\right]^{+}$. The top-down attentive excitatory modulatory AMYG input is $200\sum_{r} W_{tri}^{AM}\left[A_{ri}\right]^{+}$. The W_{tri}^{AM} are LTM weights that map US-specific AMYG categories to US-specific ORB_m cells which code reward value. The driving inhibitory off-surround RHIN and AMYG inputs are $0.2\sum_{u\neq t}\left[R_u\right]^{+}$ and $4\sum_{u\neq t}\sum_{r} W_{rui}^{AM}\left[A_{ri}\right]^{+}$, respectively. Inhibitory inputs include a recurrent inhibition between appetitive and aversive ORB_l cells, $15\sum_{j\neq i} O_{tj}^{M}$.

A.1.9 BG STM Equations. Brown et al. (1999) modeled four brain regions that cooperate to generate dopaminergic bursts and dips in response to unexpected rewards and nonreward: ventral striatal matrix cells (VS), ventral striatal striosomal cells (SD), pedunculopontine cells (PPT/LDT), and dopaminergic cells (SNc/VTA); see Fig. 1. When unexpected rewards or conditioned stimuli are presented, SNc/VTA Cells show a transient burst of activity. Cells in the PPTN/LDT drive this bursting response. Conditioned stimuli excite the PPTN/LDT via VS cells while food rewards drive PPTN/LDT cells via both LH_gus and VS inputs. CS-related inputs from the ORB_l activate SD cells. An adaptively-timed inhibitory pathway from SD cells to the SNc/VTA suppresses dopamine bursts at the expected time of reward. If an expected reward is omitted, this adaptively timed signal from SD cells to the SNc/VTA inhibits the dopamine cells, resulting in a transient dip in dopamine. Together, excitatory and inhibitory conditioning pathways through the basal ganglia act to ensure dopamine bursts and dips signal reward prediction errors.

VS STM Equations. Ventral striatal matrix cell activities are represented by activities, V_{ri}. VS cells are sensitive to US-specific value category inputs from the AMYG and learn to respond to object-value inputs from the ORB_l. Subscript *r* indicates that the *r*-th VS cell favors the *r*-th US-specific AMYG category; subscript *i* indicates affective valence. VS cells receive excitatory driving inputs from the AMYG, A_{ri} and ORB_l, O_{ji}^{L}:

$$\tfrac{1}{50}V_{ri} = -V_{ri} + (1-V_{ri})\left(20\left(\sum_{j} W_{rji}^{OV}\left[O_{ji}^{L}\right]^{+} + \left[A_{ri}-0.1\right]^{+}\right)\right) \tag{20}$$

The excitatory shunting term $(1-V_{ri})$ limits the activity of the cell to the interval [0, 1]. ORB_l inputs $20\sum_{j} W_{rji}^{OV}\left[O_{ji}^{L}\right]^{+}$ and AMYG inputs $20\left[A_{ri}-0.1\right]^{+}$ are the excitatory driving ORB_l and AMYG inputs, respectively. The W_{rji}^{OV} are LTM weights that map CS-specific ORB_l cells to US-specific VS cells, while preserving affective valence, *i*.

LDT/PPTN STM Equations. PPTN/LDT activities model the pedunculopontine and laterodorsal tegmental brainstem nuclei (Kobayashi et al., 2002). PPTN/LDT activity is described using a pair of variables, P_1 and P_2, with coupled equations. PPTN/LDT cells receive opponent, bottom-up, driving inputs from LH_gus cells, H_{si}^G and driving inputs from VS cells (Figure 5a). The effect of VS activity V_{ri} on PPTN/LDT is modeled as a net excitatory driving input because the VS inhibits the ventral pallidum and thus disinhibits the PPTN/LDT:

$$\tfrac{1}{50}\dot{P}_1 = -P_1 + (1-P_1)\left(2.5\left[\sum_s \left(H_{s1}^G - H_{s2}^G\right)\right]^+ + \sum_i \sum_r V_{ri} + 40\right) - 1500(1+P_1)\left[P_2\right]^+ \tag{21}$$

and

$$\dot{P}_2 = -P_2 + (1-P_2)\left[P_1\right]^+ . \tag{22}$$

In (21), excitatory and inhibitory shunting terms $(1-P_1)$ and $(1+P_1)$, respectively, bound PPTN/LDT activity within the interval [-1, 1]. The excitatory driving input $2.5\left[\sum_s \left(H_{s1}^G - H_{s2}^G\right)\right]^+$ gives the net appetitive signal from LH_gus cells to the PPTN/LDT. Excitatory driving inputs $\sum_i \sum_r V_{ri}$ sum VS cell activity, enabling stimuli represented in the ORB_l to excite the PPTN/LDT. An arousal input set to 40 biases PPTN cell activity. Term $1500\left[P_2\right]^+$ is a driving, inhibitory off-surround input. Term P_2 approximates the strength of a slow after-hyperpolarization process.

In (22), the after-hyperpolarization process, P_2, is driven by the "input" $(1-P_2)\left[P_1\right]^+$, where $(1-P_2)$ bounds P_2 activation to the interval [0, 1] and P_1 represents excitatory PPTN/LDT output. The strong driving inhibition arising from the afterhyperpolarizing signal P_2 is responsible for generating the phasic profile of PPTN/LDT signals P_1 (see Fig. 12).

SD STM Equations. Striosomal cells (SD) carry out an adaptive timing function that suppresses dopaminergic bursts to expected rewards. SD cells can fire at an adaptively timed delay after the onset of a CS, thereby inhibiting dopamine cells in the SNc/VTA. This delayed burst of inhibitory firing is the result of a Ca^{2+}-dependent second-messenger process governed by metabotropic glutamate receptors (mGluR) (Fiala et al., 1996; Brown et al., 1999). Activation of mGluRs causes a spike in Ca^{2+} currents that can lead to the depolarization of SD cells after a timed delay.

SD cell activity, B_{jg}, is driven by excitatory signals, O_{ji}^L, from the ORB_l. Dendritic spines that receive their driving excitatory inputs from the *j*-th ORB_l cell are indexed with the subscript, *j*. The subscript *g* indicates the *g-th* SD cell responds to ORB_l inputs at a rate characterized by the *g*-th rate parameter, β_g. Note that the subscripts *j* and *g* do not necessarily index single neurons, but pools of synapses across one or many neurons (Brown et, al., 1999):

$$\left(\frac{1}{\beta_g}\right)\dot{B}_{jg} = -B_{jg} + (1-B_{jg})\left(2.5\left[O_{j1}^L - 0.03\right]^+\right) \tag{23}$$

Where $\beta_g = \dfrac{10}{30g-23}, \quad g = \{1,\ldots,60\}.$ (24)

In (23), the excitatory shunting term $(1-B_{jg})$ bounds activity within the interval [0, 1]. ORB_I inputs $2.5\left[O_{j1}^{L}-0.03\right]^{+}$ provide the excitatory driving inputs. The rate parameters, β_g, span the range of values specified in Equation (24), providing the basis for a range of delayed cell activations and Ca^{2+} spikes.

Equations (25)-(27) describe how the activation of mGluR channels on SD cells gives rise to a rapid spike in cytosolic Ca^{2+}, $G_{jg}Y_{jg}$, driving adaptively timed SD-to-SNc/VTA inhibitory responses. Equation (25) describes how SD cell activity, B_{jg} alters the conductance of Ca^{2+} current, G_{jg}:

$$\tfrac{1}{5}\dot{G}_{jg} = -4G_{jg} + (5-G_{jg})\left(h\left(B_{jg}\right)\right), \tag{25}$$

$$\text{Where } h\left(B_{jg}\right) = \begin{cases} 1 & \text{if} \quad B_{jg}-0.2>0 \\ 0 & \text{if} \quad B_{jg}-0.2\le 0 \end{cases}. \tag{26}$$

The rate at which Ca^{2+} passes to the cytosol from endoplasmic stores is bound by the term $(5-G_{jg})$ to the interval [0, 5]. The function *h,* defined in Equation (26), is a step function that indicates SD cell activity must exceed a threshold of 0.2 in order to trigger the rapid buildup of cytosolic Ca^{2+}, $G_{jg}Y_{jg}$. As the Ca^{2+} concentration builds to maximal level, the available Ca^{2+} in both endoplasmic and local cytosolic stores, Y_{jg}, rapidly depletes. Equation (27) describes how the level of available Ca^{2+}, Y_{jg}, is decreased by a Ca^{2+} spike, $G_{jg}Y_{jg}$:

$$\tfrac{1}{1}\dot{Y}_{jg} = (1-Y_{jg}) - 40\left[G_{jg}Y_{jg}-0.2\right]^{+} \tag{27}$$

Available Ca^{2+} passively accumulates at a rate given by the term $(1-Y_{jg})$. Term $-40\left[G_{jg}Y_{jg}-0.2\right]^{+}$ describes the depletion of intracellular Ca^{2+} as a consequence of the calcium spike. Once depleted, endoplasmic and other available Ca^{2+} stores remain low for as long as the SD cell continues to receive a tonic input. Subsequent calcium spikes occur only after a recovery period has passed.

SD cells are capable of generating Ca^{2+} spikes, $G_{jg}Y_{jg}$, at a spectrum of delays after CS onset. During the peak phase of a Ca^{2+} spike, $\left[G_{jg}Y_{jg}-0.2\right]^{+}$, inhibitory transmission from SD cells to the SNc/VTA is boosted. LTM weights, Z_{jg}, (see Equation (46)) strengthen the influence of these delayed spikes on neural transmission, allowing SD cells to generate an adaptively timed output, $Z_{gj}\left[G_{jg}Y_{jg}-0.2\right]^{+}$.

SNc/VTA output STM Equations. Activities of model neurons in the dopaminergic midbrain are represented by S_1. Neurons in the SNc/VTA receive excitatory driving inputs, P_1, from PPTN/LDT cells and an adaptively timed, inhibitory input from SD cells, $Z_{gj}\left[G_{jg}Y_{jg}-0.2\right]^{+}$:

$$\tfrac{1}{50}\dot{S}_1 = -S_1 + (1-S_1)\left(10\left[P_1 - 0.03\right]^+ + \alpha_2\right) - (0.1+S_1)\left(\sum_g \sum_j Z_{jg}\left[G_{jg}Y_{jg} - 0.2\right]^+\right) \quad . \tag{28}$$

The excitatory and inhibitory shunting terms $(1-S_1)$ and $(0.1+S_1)$, respectively, bound cell activity within the interval [-0.1, 1]. Term $10\left[P_1 - 0.03\right]^+$ describes the driving excitatory input from the PPTN. Term α_2 is a tonic arousal input that ensures baseline dopamine activity is non-zero, providing some dynamic range for dopamine dips. The arousal parameter, α_2, is set equal to 0.28. The driving, inhibitory term $\sum_g \sum_j Z_{gj}\left[G_{gj}Y_{gj} - 0.2\right]^+$ represents the sum of adaptively timed signals from SD cells across all spectral delays, *g* and cue preferences, *j*. This term enables dopamine signals to be sensitive to the learned expectations of SD cells regarding the predicted occurrence of rewards and their expected time of delivery.

Dopamine reinforcement signals. The effective dopamine signal is determined using transient deviations of dopamine signals from a tonic or baseline dopamine level, S_2:

$$\tfrac{1}{5}\dot{S}_2 = S_1 - S_2 \quad . \tag{29}$$

Equation (29) has a much slower rate constant than that used in Equation (28). This allows S_2 to compute a time-average of momentary dopamine cell activity, S_1.

Transient deviations from the baseline signal S_2 constitute phasic dopamine reinforcement signals (Wickens et al., 1996). Equations (30)-(33) describe these phasic dopamine signals. Equations (30) and (31) define the effective dopamine burst, N_1, and dopamine dip, N_2, signals in the striatum:

$$N_1 = \left[S_1 - S_2 - 0.02\right]^+ \tag{30}$$

and

$$N_2 = \left[S_2 - S_1 - 0.02\right]^+ \quad . \tag{31}$$

Dopamine cell activity, S_1, elicits a dopamine burst or dip (N_1 or N_2) when it exceeds baseline dopamine activity, S_2, by an amount in excess of the threshold parameter, 0.0175. This threshold helps prevent minor fluctuations in DRIVE and GUS inputs from controlling learning.

Equations (32) and (33) define the effective dopamine burst, D_1, and dopamine dip, D_2, signals in the AMYG and ORB_l where dopamine clearance is slower than in the striatum (Garris and Rebec, 2002):

$$\tfrac{1}{3}\dot{D}_1 = -D_1 + 20N_1 \tag{32}$$

and

$$\tfrac{1}{3}\dot{D}_2 = -D_2 + 20N_2 \quad . \tag{33}$$

Terms $20N_1$ and $20N_2$ are dopamine burst and dip inputs.

A.2 Medium Term Memory Equations.

A.2.1 LH_in to LH_gus Drive Habituation. The habituating transmitter term Y_{si} gates signals from LH_in cells to LH_gus cells:

$$\tfrac{1}{1}\dot{Y}_{si} = (1 - Y_{si}) - 1.2Y_{si}\left[H_{si}^{I}\right]^{+}. \tag{34}$$

The habituative process depends on a recovery process, $(1 - Y_{si})$, and an activity-dependent depletion process, $-1.2Y_{si}\left[H_{si}^{I}\right]^{+}$. Activity-dependent depletion is driven by LH_in cell activity, H_{si}^{I}. The rate constant of Equation (34) has a value of 1, hence habituative MTM processes adapt to inputs much more slowly than do STM processes. The habituating transmitter term, Y_{si}, plays an important role generating rebound responses in the LH and gated dipole circuit (Grossberg, 1972; see Section 2.3.3). During the first phase of every task, habituating transmitter levels, Y_{si}, adapt to the tonic arousal inputs that drive the early activity of LH_in cells. When transient, stimulus-related signals activate different LH_in cells, the habituated transmitter gates of the LH_in cells become imbalanced. When an arousal burst occurs or if these transient signals are removed, the imbalanced habituative transmitter gates can persist, during which time rebound responses can result from opponent processing in the LH circuit.

A.2.2 GUS to LH_gus Taste Habituation. GUS inputs to RHIN cells, R_t, and LH_gus cells, H_{si}^{G} are gated by a habituating transmitter, X_m:

$$200\dot{X}_m = 0.01(1 - X_m) - (G_m X_m). \tag{35}$$

The habituation involves a slow recovery process, 0.01 $(1 - X_m)$ and a faster depletion process, $-(G_m X_m)$. Depletion occurs in a consumption dependent fashion and is driven by GUS inputs, G_m. The taste-specific habituation of GUS inputs, X_m, is a second mechanism of food specific satiety (FSS) that complements the model's "drive reduction" mechanism. This second mechanism of FSS can explain the observation that the kind of FSS that is assessed by actual consumption rather than by CS preference remains intact even after ORB_l and AMYG lesions (Hatfield et al., 1996; Dunn and Everitt, 1988).

A.3 Long Term Memory Equations.

A.3.1 AMYG to ORB_l *LTM Weights.* Connections from AMYG cells to ORB_l cells have LTM weights, W_{rji}^{AO}, that obey a dopamine-modulated instar learning rule (see Equation (7)). LTM weights W_{rji}^{AO} assign incentive motivation to object-value cells in the ORB_l:

$$\tfrac{1}{5}\dot{W}_{rji}^{AO} = \left[O_{ji}^{L}\right]^{+}\left[(D_1 + 0.01)\left(\left[A_{ri}\right]^{+} - W_{rji}^{AO}\right) - (D_2)2W_{rji}^{AO}\right]. \tag{36}$$

Postsynaptic ORB_l activity, $\left[O_{ji}^{L}\right]^{+}$ gates the learning and decay of LTM weights. Term $(D_1 + 0.01)\left(\left[A_{ri}\right]^{+} - W_{rji}^{AO}\right)$ describes how dopamine spikes, D_1, modulate the learning of presynaptic values, $\left[A_{ri}\right]^{+}$, by the LTM weights, W_{rji}^{AO}. In the absence of dopamine, this learning process occurs a base rate of 0.01. Term $-(D_2)2W_{rji}^{AO}$ indicates that LTM weights, W_{rji}^{AO}, decay when a dopamine dip occurs, D_2.

A.3.2 LH_out to AMYG LTM Weights. Connections from LH_out cells to AMYG cells have LTM weights, W_{rsi}^{HA}, that obey an activity-gated, steepest descent instar learning rule (see

Equation (7)). These weights gate the convergence of LH_out homeostatic signals onto US-specific drive value category cells in the AMYG:

$$8\dot{W}_{rsi}^{HA} = \left[A_{ri} - 0.027\right]^{+}\left(\left[H_{si}^{O}\right]^{+} - W_{rsi}^{HA}\right) \tag{37}$$

Term $\left[A_{ri} - 0.027\right]^{+}$ provides a postsynaptic gate on learning while the term $\left(\left[H_{si}^{O}\right]^{+} - W_{rsi}^{HA}\right)$ describes the process by which LTM weights learn to reflect the activity of LH_out cells. Term $\left[A_{ri} - 0.027\right]^{+}$ specifies that AMYG cell activity must exceed a threshold of 0.027 before learning can take place. This threshold was selected to ensure learning takes when the AMYG is activated by cortical inputs, and not simply by feedback from of the positive recurrent signal function, *g(A)*.

A.3.3 IT$_a$ to AMYG LTM Weights. Connections from IT$_a$ cells to AMYG cells have LTM weights, W_{jri}^{IA}, that follow a dopamine-modulated outstar learning rule (see Equation (7)). LTM weights W_{jri}^{IA} enable object categories represented in the IT$_a$ to acquire conditioned reinforcer properties:

$$\tfrac{1}{5}\dot{W}_{jri}^{IA} = \left[I_j\right]^{+}\left[\left(D_1 + 0.01\right)\left(\left[A_{ri}\right]^{+} - W_{jri}^{IA}\right) - \left(D_2\right)2W_{jri}^{IA}\right] \tag{38}$$

Presynaptic IT$_a$ activity, $\left[I_j\right]^{+}$, gates the learning and decay of LTM weights. Term $\left(D_1 + 0.01\right)\left(\left[A_{ri}\right]^{+} - W_{jri}^{IA}\right)$ describes how dopamine spikes, D_1, modulate the learning of postsynaptic activation, $\left[A_{ri}\right]^{+}$. In the absence of dopamine, the learning process occurs at a base rate of 0.01. Term $-\left(D_2\right)2W_{jri}^{IA}$ indicates that LTM weights decay when a dopamine dip occurs, D_2.

A.3.4 RHIN to AMYG LTM Weights. Connections from RHIN cells to AMYG cells have LTM weights, W_{tri}^{RA}, that are governed by dopamine-modulated, outstar learning (Equation (7)). LTM weights W_{tri}^{RA} enable multimodal food reward categories cells in RHIN to acquire reinforcer properties:

$$\tfrac{1}{5}\dot{W}_{tri}^{RA} = \left[R_t\right]^{+}\left[\left(D_1 + 0.01\right)\left(\left[A_{ri}\right]^{+} - W_{tri}^{RA}\right) - \left(D_2\right)2W_{tri}^{RA}\right] \tag{39}$$

Pre-synaptic RHIN cell activity $\left[R_t\right]^{+}$ gates learning and decay processes for the LTM weights, W_{tri}^{RA}. Term $\left(D_1 + 0.01\right)\left(\left[A_{ri}\right]^{+} - W_{tri}^{RA}\right)$ describes the dopamine-modulated process by which weights, W_{tri}^{RA}, come to reflect postsynaptic AMYG activity, $\left[A_{ri}\right]^{+}$. In the absence of dopamine, this process takes place at a rate of 0.01. Term $-\left(D_2\right)2W_{tri}^{RA}$ indicates dopamine dips induce the decay of LTM weights.

A.3.5 AMYG to LH_out LTM Equations. Connections from AMYG cells to LH_out cells have LTM weights, W_{sri}^{AH}, that obey an activity-gated, steepest-descent outstar learning law (see

Equation (6)). LTM weights W_{sri}^{AH} enable US-specific drive value categories in the AMYG to excite drive cells in the LH activated by the consumption of specific food rewards:

$$8\dot{W}_{sri}^{AH} = \left[A_{ri} - 0.027\right]^{+} \left(\left[H_{si}^{O}\right]^{+} - W_{sri}^{AH}\right). \tag{40}$$

Term $\left[A_{ri} - 0.027\right]^{+}$ provides a presynaptic gate on learning. Term $\left(\left[H_{si}^{O}\right]^{+} - W_{sri}^{AH}\right)$ describes the process by which LTM weights learn to reflect LH_out cell activity, H_{si}^{O}. Term $\left[A_{ri} - 0.027\right]^{+}$ specifies that AMYG cell activity must exceed a threshold of 0.027 before learning can take place. This process allows LTM weights W_{sri}^{AH} to learn to encode a prototype of the metabolic activations in the LH associated with US consumption.

A.3.6 AMYG to ORB_m *LTM Equations* Connections from AMYG cells to ORB_m cells have LTM weights, W_{rti}^{AM}, that obey a dopamine-modulated instar learning rule (Equation (7)). LTM weights W_{rti}^{AM} assign incentive motivational value to food rewards represented in the ORB_m:

$$\tfrac{1}{5}\dot{W}_{rti}^{AM} = \left[O_{ti}^{M}\right]^{+} \left[\left(D_1 + 0.01\right)\left(\left[A_{ri}\right]^{+} - W_{rti}^{AM}\right) - \left(D_2\right)2W_{rti}^{AM}\right]. \tag{41}$$

Postsynaptic ORB_m activity, $\left[O_{ti}^{M}\right]^{+}$, gates learning and decay. Term $\left(D_1 + 0.01\right)\left(\left[A_{ri}\right]^{+} - W_{rti}^{AM}\right)$ indicates dopamine bursts modulate the learning of presynaptic activity, $\left[A_{ri}\right]^{+}$, by LTM weights, W_{rti}^{AM}. The term $-\left(D_2\right)2W_{rti}^{AM}$ indicates that LTM weights decay when a dopamine dip occurs, D_2.

A.3.7 ORB_l *to VS LTM Equations.* Connections from ORB_l cells to VS cells have LTM weights, W_{jri}^{OV}, that obey a dopamine-gated instar rule (Brown et al., 2004; Equation (7)). LTM weights W_{jri}^{OV} allow conditioned stimuli to strongly activate dopaminergic responses:

$$\tfrac{1}{10}W_{jri}^{OV} = V_{ri}\left[N_1(2.5O_{ji}^{L} - W_{jri}^{OV}) - 0.2N_2W_{jri}^{OV}\right]. \tag{42}$$

Post-synaptic VS activity, V_{ri}, gates learning and decay. Term $N_1(2.5O_{ji}^{L} - W_{jri}^{OV})$ indicates that dopamine bursts, N_1, doubly gate steepest descent learning. LTM weights W_{jri}^{OV} learn to reflect the value of postsynaptic ORB_l cells, $2.5O_{ji}^{L}$. Term $-0.2N_2W_{jri}^{OV}$ indicates that dopamine dips, N_2, gate weight decay.

A.3.8 Adaptive Timing LTM Equations. Adaptive LTM weights Z_{jg} determine the strength of timed inhibitory outputs from SD cells to the SNc/VTA. These LTM weights, Z_{jg}, adapt according to an equation similar to dopamine-gated steepest descent:

$$\tfrac{1}{300}\dot{Z}_{jg} = \left[G_{jg}Y_{jg} - 0.2\right]^{+}\left(N_1 - Z_{jg}N_2\right). \tag{43}$$

Term $\left[G_{jg}Y_{jg} - 0.2\right]^{+}$ gates learning, ensuring learning occurs only during the peak phase of a Ca^{2+} spike in an SD cell. Term $\left(N_1 - Z_{jg}N_2\right)$ describes the process by which weights, Z_{jg} grow

when dopamine spikes are present and decay when dopamine dips are present. The growth and decay of LTM weights, Z_{jg}, tracks reward history, inhibiting dopamine responses to predictable rewards. This ensures dopamine signals generated by the SNc/VTA reflect a reward prediction error.

A.3.9 ITA to FEF LTM Weights. Connections from ITA cells to the FEF have LTM weights, W_j^{IF}, that follow a dopamine-modulated outstar learning rule (see Equation (7)). LTM weights W_j^{IF} enable object categories represented in the ITA to elicit saccades using stimulus-response learning:

$$\tfrac{1}{5}\dot{W}_j^{IF} = \left[I_j\right]^+ \left[\left(D_1 + 0.01\right)\left(F_j - W_j^{IF}\right) - \left(D_2\right)2W_j^{IF}\right] \quad . \tag{44}$$

Presynaptic IT_a activity, $\left[I_j\right]^+$, gates the learning and decay of LTM weights. Term $\left(D_1 + 0.01\right)\left(F_j - W_j^{IF}\right)$ describes how dopamine spikes, D_1, modulate the learning of FEF activation, F_j. In the absence of dopamine, the learning process occurs at a base rate of 0.01. Term $-\left(D_2\right)2W_j^{IF}$ indicates that LTM weights decay when a dopamine dip occurs, D_2.

A.3.10 RHIN to CMA LTM Weights. Connections from RHIN cells to the CMA have LTM weights, W_t^{RZ}, that follow a dopamine-modulated outstar learning rule (see Equation (7)). LTM weights W_t^{RZ} enable US categories represented in the RHIN to drive consumption through stimulus-response learning:

$$\tfrac{1}{5}\dot{W}_t^{RZ} = \left[R_t\right]^+ \left[(D_1 + 0.01)(Z_t - W_t^{RZ}) - (D_2)2W_t^{RZ}\right] \quad . \tag{45}$$

Presynaptic ITA activity, $\left[R_t\right]^+$, gates the learning and decay of LTM weights. Term $(D_1 + 0.01)(Z_t - W_t^{RZ})$ describes how dopamine spikes, D_1, modulate the learning of FEF activation, Z_t. In the absence of dopamine, the learning process occurs at a base rate of 0.01. Term $-(D_2)2W_t^{RZ}$ indicates that LTM weights decay when a dopamine dip occurs, D_2.

A.4 Outputs.

A.4.1 Blood Pressure Output. The blood pressure response, BPR, is influenced by appetitive and aversive stimuli (Braesicke, et al. 2005). This influence is relayed from the hypothalamus to cardiovascular regulatory neurons in the medulla (Smith et al., 1990; Nakamura et al., 1992; Zhang et al., 2005, 2006). The component of the blood pressure variable attributable to appetitive or aversive stimuli, B, is calculated as follows:

$$\dot{B} = -B + 15\sum_i \left[H_{si}^O - \tfrac{1}{4}\sum_{s=1}^{4} H_{si}^O\right]^+, \tag{46}$$

Where $BPR = 120 + B$. (47)

The term $15\sum_i \left[H_{si}^O - \tfrac{1}{4}\sum_{s=1}^{4} H_{si}^O\right]^+$ relays excitatory information from LH_out cells regarding stimuli and rewards. The blood pressure response, BPR, reflects the integral of the LH input added to a baseline blood pressure level of 120.

A.4.2 Saccadic Output. Saccadic responses are generated by object category-selective cells in the FEF. In vivo, the FEF receives projections from both the ORB_l and IT_a (Barbas,

1992; Bullier et al., 1996). Correspondingly, in the model, FEF cells integrate inputs from the ORB_l and IT_a along with arousal inputs. When an FEF cell activity F_j exceeds a threshold of 0.3, a saccade was elicited in response to the corresponding cue. Only one saccade could be elicited per trial:

$$10\dot{F}_j = -F_j + 4\left[O_{j1}\right]^+ + \left[I_j\right]^+ + \alpha_3 + \varepsilon_j. \quad (48)$$

Activity F_j passively decays at rate 1 via term $-F_j$. Additive excitatory terms $4\left[O_{j1}\right]^+$ and $\left[I_j\right]^+$ describe inputs that arise from the ORB_l and IT_a. Terms α_3 and ε_j are constants that take on non-zero values during stimulus presentation.

Term α_3 is an arousal input that activates the FEF depending on whether or not an instrumental response is required to gain reward. For the SVD Task where the CS was presented for 450 ms before a saccade was made, α_3 = 6.5. For the Pavlovian CS Task for which the CS was presented for 2 seconds, α_3 = 0. This arousal term helps to realize the different response and timing requirements of the CS and SVD tasks. In the CS task, α_3=0 because responses are incidental to the acquisition of reward and may be generated anytime across the 2 second CS presentation time, or not at all. For the SVD task, a response must be made within 400 ms in order to gain reward. The choice of α_3= 6.5 ensures that a decision is made within this time frame.

The noise terms ε_j are constants that break symmetry during decision-making. Values for ε_j are randomly selected at the start of each trial from a uniform distribution over the interval [0, 1]. The noise terms acknowledge that signals from unknown sources can influence behavior and decision-making, generating behavioral variation or breaking the symmetry between closely matched options. In tasks such as the SVD reversal task, where stimulus and response contingencies change, the response variability introduced by the term, ε_j, can drastically speed the learning of new associations.

In essence, model FEF cells function as cumulative spike counters, integrating ORB_l and IT_a activity along with some noise and arousal inputs to elicit saccades using a "race to threshold" rule (Schall and Thompson, 1999). For a more detailed representation of the FEF, see Brown et al. (2004). Parameter values were selected to ensure reaction times during the SVD task fall between 300ms and 450ms and that no responses are made in the CS task prior to learning taking place. IT_a inputs play a critical role in driving saccadic behavior when ORB_l inputs are silent or after ORB_l has been lesioned.

A.4.3 Consumption Output. Food consumption responses are generated using signals from premotor cortical mouth area cells CMA cells:

$$\dot{Z}_t = -Z_t + W_t^{RZ} R_t + M_{t1}. \quad (49)$$

Term M_{t1} is the appetitive ORB_m activity, associated with the *t-th* US. $W_t^{RZ} R_t$ are the learned RHIN inputs to the CMA. Z_t is the analog strength of the consumption response.

REFERENCES

Amaral, D.G., Price, J.L., 1984. Amygdalo-cortical projections in the monkey (Macaca fascicularis). J Comp Neurol. 230, 465-496.

Balleine, B.W., Dickinson, A., 1998. Goal-directed instrumental action: Contingency and incentive learning and their cortical substrates. Neuropharmacology. 37, 407-419.

Balleine, B.W., Killcross, S., 1994. Effects of ibotenic acid lesions of the nucleus accumbens on instrumental action. Behav Brain Res. 65, 181-193.

Balleine, B.W., Garner, C., Gonzalez, F., Dickinson, A., 1995. Motivational control of heterogeneous instrumental chains. J Exp Psychol: Anim Beh Proc. 21, 203-217.

Barbas, H., 1995. Pattern in the cortical distribution of prefrontally directed neurons with divergent axons in the rhesus monkey. Cereb Cortex. 5, 158-165.

Baxter, M.G., Parker, A., Lindner, C.C., Izquierdo, A.D., Murray, E.A., 2000. Control of response selection by reinforcer value requires interaction of amygdala and orbital prefrontal cortex. J Neurosci. 20, 4311-4319.

Baylis, L.L., Gaffan, D., 1991. Amygdalectomy and ventromedial prefrontal ablation produce similar deficits in food choice and in simple object discrimination learning for an unseen reward. Exp Brain Res. 86, 617-622.

Bechara, A., Damasio, H., Damasio A.R., Lee, G.P., 1999. Different contributions of the human amygdala and ventromedial prefrontal cortex to decision-making. J Neurosci. 19, 5473-5481.

Belova, M.A., Patton, J.J., Morrison, S.E., Salzman, C.D. 2007. Neuron expectation modulates neural responses to pleasant and aversive stimuli in primate amygdala. Neuron. 55, 970-980.

Bernardis, L.L., Bellinger, L.L., 1996. The lateral hypothalamic area revisited: Ingestive behavior. Neurosci Biobehav Rev. 20, 189-287.

Braesicke, K., Parkinson, J.A., Reekie, Y., Man, M.S., Hopewell, L., Pears, A., Crofts, H., Schnell, C.R., Roberts, A.C., 2005. Autonomic arousal in an appetitive context in primates: A behavioural and neural analysis. Eur J Neurosci. 21, 1733-1740.

Brown, J.W., Bullock, D., Grossberg, S., 1999. How the basal ganglia use parallel excitatory and inhibitory learning pathways to selectively respond to unexpected rewarding cues. J Neurosci. 19, 10502-10511.

Brown, J.W., Bullock, D., Grossberg, S., 2004. How laminar frontal cortex and basal ganglia circuits interact to control planned and reactive saccades. Neural Netw. 17, 471-510.

Brown, T.H., Kairiss, E.W., Keenan, C.L., 1990. Hebbian synapses: Biophysical mechanisms and algorithms. Annu Rev Neurosci. 13, 475-511.

Bunge, S.A.,Wallis, J.D., Parker, A., Brass, M., Crone, E.A., Hoshi, E., Sakai, H. (2005). Neural circuitry underlying rule use in humans and nonhuman primates. J Neurosci, 25, 10347–10350.

Cardinal, R.N., Parkinson, J.A., Hall, J., Everitt, B.J., 2002. Emotion and motivation: The role of the amygdala, ventral striatum, and prefrontal cortex. Neurosci Biobehav Rev. 26, 321-352.

Carpenter, G.A., Grossberg, S., 1991. Pattern Recognition by Self-Organizing Neural Networks. MIT Press, Cambridge MA.

Corbit, L.H., Balleine, B.W., 2003. Instrumental and Pavlovian incentive processes have dissociable effects on components of a heterogenous instrumental chain. J Exp Psych Anim Behav Process. 29, 99-106.

Corbit, L.H., Balleine, B.W., 2005. Double dissociation of basolateral and central amygdala lesions on the general and outcome-specific forms of pavlovian-instrumental transfer. J Neurosci. 25, 962-70.

Davidson, T.L., Altizer, A.M., Benoit, S.C., Walls, E.K., Powley, T.L., 1997. Encoding and selective activation of "metabolic memories" in the rat. Behav Neurosci. 111, 1014-1030.

Dickinson, A., Dearing, M.F., 1979. Appetitive-Aversive Interactions and Inhibitory Processes. Erlbaum, Hillsdale NJ.

Dickinson, A., Balleine, B.W., 2001. The role of learning in the operation of motivational systems. In Steven's Handbook Of Experimental Psychology, 3rd Edition, H.E. Pashler, R. Gallistel, eds. John Wiley & Sons, New York, pp 497-533.

Dranias, M.R., Bullock, D., Grossberg, S., 2007. Emotional and behavioral responses to the devaluation of stimuli by satiation: A computational model. Computational and Systems Neuroscience. Poster Presentation III-68.

Dranias, M.R., Bullock, D., Grossberg, S., 2007. Neural Dynamics of Conditioning and Outcome-Specific Revaluation: Cortical, Amygdala, Hypothalamic, and Basal Ganglia. Interactions Eleventh International Conference on Cognitive and Neural Systems. Slide Presentation.

Dunn, L.T., Everitt, B.J., 1988. Double dissociations of the effects of amygdala and insular cortex lesions on conditioned taste aversion, passive avoidance, and neophobia in the rat using the excitotoxin ibotenic acid. Behav Neurosci. 102, 3-23.

Easton, A., Gaffan, D., 2000. Comparison of perirhinal cortex ablation and crossed unilateral lesions of the medial forebrain bundle from the inferior temporal cortex in the rhesus monkey: Effects on learning and retrieval. Behav Neurosci. 114, 1041-1057.

Fiala, J.C., Grossberg, S., Bullock, D., 1996. Metabotropic glutamate receptor activation in cerebellar Purkinje cells as substrate for adaptive timing of the classically conditioned eye-blink response. J Neurosci. 16, 3760-3774.

Fiorillo, C.D., Tobler, P.N., and Schultz, W., 2003. Discrete coding of reward probability and uncertainty by dopamine neurons. Science. 299, 1899-1902.

Frank, M.J., Claus, E.D., 2006. Anatomy of a decision: Striato-orbitofrontal interactions in reinforcement learning, decision making, and reversal. Psychol Rev. 113, 300-326.

Fukuda, M., Ono, T., Nakamura, K., 1987. Functional relations among inferotemporal cortex, amygdala, and lateral hypothalamus in monkey operant feeding behavior. J Neurophysiol. 57, 1060-1077.

Gallagher, M., McMahan, R.W., Schoenbaum, G. 1999. Orbitofrontal cortex and representation of incentive value in associative learning. J Neurosci. 19, 6610-6614.

Garris, P.A., Rebec, G.V., 2002. Modeling fast dopamine neurotransmission in the nucleus accumbens during behavior. Behav Brain Res. 137, 47-63.

Grossberg, S., 1968. Some nonlinear networks capable of learning a spatial pattern of arbitrary complexity. Proc. Natl. Acad. Sci. 59, 368-372.

Grossberg, S., 1971. On the dynamics of operant conditioning. J Theor Biol. 33, 225-255.

Grossberg, S., 1972. A neural theory of punishment and avoidance, II: Quantitative theory. Math Biosci. 15, 253-285.

Grossberg, S., 1973. Contour enhancement, short-term memory, and constancies in reverberating neural networks. S App Math. 52**,** 213-257.

Grossberg, S., 1975. A neural model of attention, reinforcement and discrimination learning. Int Rev Neurobiol. 18, 263-327.

Grossberg, S., 1980. How does a brain build a cognitive code? Psychol Rev. 87, 1-51.

Grossberg, S., 1982. Processing of expected and unexpected events during conditioning and attention: A psychophysiological theory. Psych Rev. 89, 529-572.

Grossberg, S., 1984. Some psychophysiological and pharmacological correlates of a developmental, cognitive, and motivational theory. In R. Karrer, J. Cohen, and P. Tueting eds. Brain and information: Event related potentials . New York : New York Academy of Sciences, pp 58-142.

Grossberg S., 1999. Neural models of normal and abnormal behavior: what do schizophrenia, parkinsonism, attention deficit disorder, and depression have in common? In Progress in Brain Research, Volume 121. J.A. Reggia. E. Ruppin and D. Glanzman, eds. Elsevier Science, New York, pp 375-406.

Grossberg, S., 2000. The imbalanced brain: From normal behavior to schizophrenia. Biol Psychiatry. 48, 81-98.

Grossberg, S., 2005. Linking attention to learning, expectation, competition, and consciousness. In Neurobiology of attention. Itti, L., Rees, G. J.T., eds. San Diego: Elsevier. p 652.

Grossberg, S., Levine, D.S., 1987. Neural dynamics of attentionally modulated Pavlovian conditioning: Blocking, inter-stimulus interval, and secondary reinforcement. App Optics. 26, 5015-5030.

Grossberg, S., Pearson, L.R., 2007. Laminar cortical dynamics of cognitive and motor working memory, sequence learning and performance: Toward a unified theory of how the cerebral cortex works. Psychol Rev., in press.

Grossberg, S., Schmajuk, N.A., 1987. Neural dynamics of attentionally modulated pavlovian conditioning: Conditioned reinforcement, inhibition, and opponent processing. Psychobiol. 15, 195-240.

Grossberg, S., Seidman, D. 2006. Neural dynamics of autistic behaviors: Cognitive, emotional, and timing substrates. Psychol Rev. 113, 483-525.

Hall, G., 2001. Conditioning. In Steven's Handbook of Experimental Psychology, H.E. Pashler, ed. John Wiley & Sons, New York, pp 4-40.

Hanes, D.P., Patterson, W.F. II, Schall, J.D., 1998. Role of frontal eye fields in countermanding saccades: Visual, movement, and fixation activity. J Neurophys. 79, 817-834.

Hatanaka, N., Tokuno, H., Nmbu, A., Takada, M., 2000. Direct projections from the magnocellular division of the basal nucleus of the amygdala to the principal part of the cortical masticatory area in the macaque monkey. Brain Research 854: 220-223.

Hatfield, T., Han, J.S., Conley, M., Gallagher, M., Holland, P., 1996. Neurotoxic lesions of basolateral, but not central, amygdala interfere with pavlovian second-order conditioning and reinforcer devaluation effects. J Neurosci. 16, 5256-5265.

Hikosaka, O., Wurtz, R.H., 1989. The basal ganglia. In The Neurobiology of Sacccadic Eye Movements, R.Wurtz and M. Goldberg, eds. Amsterdam: Elsevier. pp 257-281.

Hodgkin, A.L., Huxley, A.F., 1952. A quantitative description of membrane current and its application to conduction and excitation in nerve. J Physiol. 117, 500-544.

Holland, P.C., Gallagher, M. 1999. Amygdala circuitry in attentional and representational processes. Trends Cogn Sci. 3, 65-73.

Hollerman, J.R., Schultz, W., 1998. Dopamine neurons report an error in the temporal prediction of reward during learning. Nat. Neurosci. 1, 304–309.

Hosokawa, T., Kato, K., Inoue, M., Mikami, A., 2004. Neurons in the orbitofrontal cortex code both visual shapes and reward types. Neuroreport. 15, 1493-1496.

Huang, C.S., Huraba, H., Murray, G.M., Sessle, B.J. 1989. Topographical distribution and functional properties of cortically induced rhythmical jaw movements in the monkey (Macaca fascicularis). J Neurophys. 61, 635-650.

Izquierdo, A., Suda, R.K., Murray, E.A. 2004. Bilateral orbital prefrontal cortex lesions in rhesus monkeys disrupt choices guided by both reward value and reward contingency. J Neurosci. 24, 7540-7548.

Jagadeesh, B., Chelazzi, L., Mishkin, M., Desimone, R., 2001. Learning increases stimulus salience in anterior inferior temporal cortex of the macaque. J Neurophys. 86, 290-303.

Kahneman, D., Tversky, A., 1979. Prospect theory: An analysis of decision under risk. Econometrica. 47, 263-291.

Kalaska, J.F., Crammond, D.J., 1995. Deciding not to GO: Neuronal correlates of response selection in a GO/NOGO task in primate premotor and parietal cortex. Cereb Cortex. 5, 410-428.

Kamin, L.J., 1969. Predictability, surprise, attention, and conditioning. In Punishment and Aversive Behavior. Campbell, B.A., Church, R. M., eds. Appleton-Century-Crofts. New York.

Karadi, Z., Oomura, Y., Nishino, H., Scott, T.R., Lenard, L., Aou, S., 1992. Responses of lateral hypothalamic glucose-sensitive and glucose-insensitive neurons to chemical stimuli in behaving rhesus monkeys. J Neurophys. 67, 389-400.

Kobayashi, Y., Inoue, Y., Yamamoto, M., Isa, T., Aizawa, H., 2002. Contribution of pedunculopontine tegmental nucleus neurons to performance of visually guided saccade tasks in monkeys. J Neurophys. 88, 715-731.

Ljungberg, T., Apicella, P., Schultz, W., 1992. Responses of monkey dopamine neurons during learning of behavioral reactions. J Neurophys. 67, 145-163.

Malkova, L., Gaffan, D., Murray, E.A., 1997. Excitotoxic lesions of the amygdala fail to produce impairment in visual learning for auditory secondary reinforcement but interfere with reinforcer devaluation effects in rhesus monkeys. J Neurosci. 17, 6011-6020.

Mirenowicz, J., Schultz, W., 1994. Importance of unpredictability for reward responses in primate dopamine neurons. J Neurophys. 72, 1024-1027.

Munoz, D.P., Wurtz, R.H., 1993. Fixation cells in monkey superior colliculus I. Characteristics of cell discharge. J Neurophys. 70, 559-575.

Munoz, D.P., Wurtz, R.H., 1995. Saccade-related activity in monkey superior colliculus I. Characteristics of burst and buildup cells. J Neurophys. 73, 2313-2333.

Muramoto, K., Ono, T., Nishijo, H., Fukuda, M., 1993. Rat amygdaloid neuron responses during auditory discrimination. Neurosci. 52, 621-636.

Murray, E.A., Gaffan, E.A., Flint, R.W., Jr., 1996. Anterior rhinal cortex and amygdala: Dissociation of their contributions to memory and food preference in rhesus monkeys. Behav Neurosci. 110, 30-42.

Nakamura, K., Ono, T., Tamura, R., 1987. Central sites involved in lateral hypothalamus conditioned neural responses to acoustic cues in the rat. J Neurophys. 58, 1123-1148.

Nakamura, K., Ono, T., Fukuda, M., Uwano, T., 1992. Paraventricular neuron chemosensitivity and activity related to blood pressure control in emotional behavior. J Neurophys. 67, 255-264.

Nishijo, H., Ono, T., Nishino, H., 1988a. Single neuron responses in amygdala of alert monkey during complex sensory stimulation with affective significance. J Neurosci. 8, 3570-3583.

Nishijo, H., Ono, T., Nishino, H., 1988b. Topographic distribution of modality-specific amygdalar neurons in alert monkey. J Neurosci. 8, 3556-3569.

Ono, T., Nakamura, K. 1985. Learning and integration of rewarding and aversive stimuli in the rat lateral hypothalamus. Brain Res. 346, 368-373.

Ono, T., Nakamura, K., Nishijo, H., Fukuda, M., 1986a. Hypothalamic neuron involvement in integration of reward, aversion, and cue signals. J Neurophys. 56, 63-79.

Parker, A., Gaffan, D., 1998. Lesions of the primate rhinal cortex cause deficits in flavour-visual associative memory. Behav Brain Res. 93, 99-105.

Pavlov, I.P., 1927. Conditioned Reflexes. Oxford University Press. Oxford. (Reprinted 1960 by Dover. New York.)

Pears, A., Parkinson, J.A., Hopewell, L., Everitt, B.J., Roberts, A.C., 2003. Lesions of the orbitofrontal but not medial prefrontal cortex disrupt conditioned reinforcement in primates. J Neurosci. 23, 11189-11201.

Pickens, C.L., Saddoris, M.P., Setlow, B., Gallagher, M., Holland, P.C., Schoenbaum, G., 2003. Different roles for orbitofrontal cortex and basolateral amygdala in a reinforcer devaluation task. J Neurosci. 23, 11078-11084.

Raizada, R.D., Grossberg, S., 2003. Towards a theory of the laminar architecture of cerebral cortex: computational clues from the visual system. Cereb Cortex. 13, 100-113.

Rescorla, R., 1991. Associative relations in instrumental learning: The eighteenth Bartlett Memorial Lecture. Q J Exp Psych. 43, 1-23.

Roesch, M.R., Olson, C.R., 2003. Impact of expected reward on neuronal activity in prefrontal cortex, frontal and supplementary eye fields and premotor cortex. J Neurophys. 90, 1766-1789.

Roesch, M.R., Olson, C.R., 2004. Neuronal activity related to reward value and motivation in primate frontal cortex. Science. 304, 307-310.

Rolls, E.T., 2000. The orbitofrontal cortex and reward. Cereb Cortex. 10, 284-294.

Rolls, E.T., Rolls, J.H., 1997. Olfactory sensory-specific satiety in humans. Phys Behav. 61, 461-473.

Rolls, E.T., Critchley, H.D., Mason, R., Wakeman, E.A., 1996. Orbitofrontal cortex neurons: Role in olfactory and visual association learning. J Neurophys. 75, 1970-1981.

Schall, J.D., 1991. Neuronal activity related to visually guided saccades in the frontal eye fields of rhesus monkeys: Comparison with supplementary eye fields. J Neurophys. 66, 559-579.

Schall, J.D., Thompson, K.G., 1999. Neural selection and control of visually guided eye movements. Annu Rev Neurosci. 22, 241-259.

Schall, J.D., Morel, A., King, D.J., Bullier, J., 1995a. Topography of visual cortex connections with frontal eye field in macaque: convergence and segregation of processing streams. J Neurosci. 15, 4464-4487.

Schall, J.D., Hanes, D.P., Thompson, K.G., King, D.J., 1995b. Saccade target selection in frontal eye field of macaque. I. Visual and premovement activation. J Neurosci. 15, 6905-6918.

Schlag, J., Schlag-Rey, M., 1987. Evidence for a supplementary eye field. J Neurophys. 57, 179-200.

Schoenbaum, G., Setlow, B., Saddoris, M.P., Gallagher M., 2003. Encoding predicted outcome and acquired value in orbitofrontal cortex during cue sampling depends upon input from basolateral amygdala. Neuron. 39, 855-867.

Schultz, W., 1998. Predictive reward signal of dopamine neurons. J Neurophys. 80, 1–27.

Schultz, W., 2007. Behavioral dopamine signals. Trends Neurosci. 30, 203-210.

Setlow, B., Gallagher, M., Holland, P.C., 2002a. The basolateral complex of the amygdala is necessary for acquisition but not expression of CS motivational value in appetitive Pavlovian second-order conditioning. Eur J Neurosci. 15, 1841-1853.

Setlow, B., Holland, P.C., Gallagher, M., 2002b. Disconnection of the basolateral amygdala complex and nucleus accumbens impairs appetitive Pavlovian second-order conditioned responses. Behavioral Neuroscience. 116, 267-275.

Sikdar, S.K., Oomura, Y. 1985. Selective inhibition of glucose-sensitive neurons in rat lateral hypothalamus by noxious stimuli and morphine. J Neurophys. 53, 17-31.

Smith, O.A., DeVito, J.L., Astley, C.A., 1990. Neurons controlling car.diovascular responses to emotion are located in lateral hypothalamus-perifornical region. Am J Physiol. 259, R943-954.

Swanson, L.W., 2000. Cerebral hemisphere regulation of motivated behavior. Brain Res. 886, 113-164.

Torii, K., Kondoh, T., Mori, M., Ono, T., 1998. Hypothalamic control of amino acid appetite. Ann N Y Acad Sci. 855, 417-425.

Toyomitsu Y., Nishijo H., Uwano T., Kuratsu J., Ono T., 2002. Neuronal responses of the rat amygdala during extinction and reassociation learning in elementary and configural associative tasks. European Journal of Neuroscience. Vol. 15: 753-768.

Tremblay, L., Schultz, W., 2000b. Reward-related neuronal activity during go-nogo task performance in primate orbitofrontal cortex. J Neurophysiol. 83, 1864-1876.

Turner, R.S., Anderson, M.E., 1997. Pallidal discharge related to the kinematics of reaching movements in two dimensions. J Neurophys. 77, 1051-1074.

Waelti, P., Dickinson, A., Schultz, W. 2001. Dopamine responses comply with basic assumptions of formal learning theory. Nature. 412, 43-48.

Weiss, S.J., Thomas, D.A., Weissman, R.D., 1996. Combining operant-baseline-derived conditioned excitors and inhibitors from the same and different incentive classes: An investigation of appetitive-aversive interactions. Q J Exp Psychol B. 49, 357-381.

Wichmann, T., Bergman, H., DeLong, M.R., 1994. The primate subthalamic nucleus. I. Functional properties in intact animals. J Neurophys. 72, 494-506.

Wickens, J.R., Begg, A.J., Arbuthnott, G.W., 1996. Dopamine reverses the depression of rat corticostriatal synapses which normally follows high-frequency stimulation of cortex in vitro. Neurosci. 70, 1-5.

Yonemori, M., Nishijo, H., Uwano, T., Tamura, R., Furuta, I., Kawasaki, M., Takashima, Y., Ono, T., 2000. Orbital cortex neuronal responses during an odor-based conditioned associative task in rats. Neuroscience. 95, 691-703.

Zhang, S., Blache, D., Vercoe, P.E., Adam, C.L., Blackberry, M.A., Findlay, P.A., Eidne, K.A., Martin, G.B., 2005. Expression of orexin receptors in the brain and peripheral tissues of the male sheep. Regul Pept. 124, 81-87.

Zhang, W., Sakurai, T., Fukuda, Y., Kuwaki, T., 2006. Orexin neuron-mediated skeletal muscle vasodilation and shift of baroreflex during defense response in mice. Am J Physiol Regul Integr Comp Physiol. 290, R1654-1663.